GENERAL ATOMIC

DIVISION OF GENERAL DYNAMICS

GA-4797

RADIATION EFFECTS ON SILICON SOLAR CELLS

by

V. A. J. van Lint, J. W. Harrity, D. K. Nichols,
and D. P. Snowden

TECHNICAL SUMMARY REPORT

May 16, 1963 through October 15, 1963

Contract NAS7-91
National Aeronautics and Space Administration

December 4, 1963

GENERAL ATOMIC

DIVISION OF

GENERAL DYNAMICS

JOHN JAY HOPKINS LABORATORY FOR PURE AND APPLIED SCIENCE

P.O. BOX 608. SAN DIEGO 12. CALIFORNIA

GA-4797

RADIATION EFFECTS ON SILICON SOLAR CELLS

TECHNICAL SUMMARY REPORT

May 16, 1963 through October 15, 1963

Work done by:

S. J. Black
S. K. Boehm
C. M. Faulkner
J. W. Harrity
N. Hubble
D. K. Nichols
D. P. Snowden
V. A. J. van Lint
E. G. Wikner
J. H. Wilson

Report written by:

V. A. J. van Lint
J. W. Harrity
D. K. Nichols
D. P. Snowden

Contract NAS7-91
National Aeronautics and
Space Administration
General Atomic Project No. 258

December 4, 1963

CONTENTS

FIGURES

1. INTRODUCTION

This Technical Summary Report describes research performed during the period of May 16, 1963 through October 15, 1963 on NASA contract NAS7-91, "Radiation Effects on Silicon Solar Cells." The work accomplished during this period includes:

a. Measurement of excess carrier recombination in semiconductor samples over a range of excess carrier concentrations varying between 10^{2} and 10^{-4} times the equilibrium majority carrier concentration.

b. Measurement of the excess carrier lifetime as a function of excess carrier concentration both before and after irradiation in 7 ohm-cm n-type silicon and in a 7 ohm-cm p-type sample. Data on the p-type sample are still being reduced.

c. Measurement by electron spin resonance (ESR) techniques of the rate of production of A centers in silicon as a function of electron energy and a search by ESR techniques for other dominant resonance lines, particularly those which might be associated with the predominant recombination center.

d. Reanalysis of the data generated previously on rate of change of mobility with irradiation to determine the net rate of introduction of ionized impurity centers.

e. Theoretical investigation of the statistics of electron-hole recombination for a single defect having two energy levels such that the second one is available only if the first one is already occupied.

The results of the work in each of these areas are described herein.

2. EXCESS CARRIER LIFETIME STUDIES

2.1 Sample Preparation

These experiments used 10 ohm-cm floating-zone-grown silicon purchased from Merck and Company. The n-type material was P-doped and the p-type was B-doped.

These materials were sliced into rectangular bars measuring approximately 20 x 2.5 x 2.5 mm and lapped with 600, 400, 2/0 and 4/0 emery paper. They were then etched for two minutes in a solution consisting of equal parts of glacial acetic, concentrated nitric, and hydrofluoric acids. From this point, treatment of the two materials differed.

For the n-type material, small As-doped gold pellets were fused to the sample at the positions where the voltage probes were desired in an oven in a forming gas atmosphere (10% H_2, 90% N_2) at 450°C. The ends of the sample were then lapped with 600-grit emery paper and electroplated with nickel. Copper leads were attached to the ends and to the gold buttons with a low-melting-temperature soft solder. A Cu-Constantan thermocouple was also soldered to one end.

The p-type sample current contacts and thermocouple were attached in the same manner as those for the n-type samples, but a different method was used to make the voltage probe contacts. The fused gold contacts used for the n-type material were found to be too highly rectifying with the p-type material, even though Ga-doped gold was used. Phosphor-bronze point probes worked best, although they too are highly rectifying at lower temperatures. The performance of these point probes is improved somewhat by the application of a contacting material* at the point of contact, but at liquid nitrogen temperature, they still have very-high-resistance contacts.

These samples were mounted in the sample chamber illustrated in Figure 2 of Reference 1.

---

*Viking L5232 Contacting Material, Victor King Materials Laboratory, Palo Alto, California.

2.2 Electronic Techniques and Equipment

Previous recombination experiments at intermediate injection levels used a small dc current through the sample with a series resistance high enough to maintain the current constant during injection. Thus to obtain recombination rates it was sufficient to merely monitor the change in voltage induced by the carrier injection. However, when one wishes to investigate recombination rates at very low or very high injection levels, more sophisticated methods must be employed.

To obtain gain for the low injection region, higher currents are used, which must be applied in pulses to avoid heating the sample. With the use of high currents, large series resistors providing constant current conditions are no longer feasible and the change in current during injection must also be monitored. To see in detail the small injection signals superimposed on the large pulses, the voltage and current signals must be clamped to ground potential until just before the linear accelerator (Linac) injection pulse. This is necessary to avoid saturating the amplifiers at the high gain positions used to observe the injection and subsequent decay.

At high injection levels, the situation is somewhat different. To investigate the early portion of the decay, high gain must be used since the voltage signal is greatly reduced due to the injected additional carriers. Thus, the high current pulse cannot be started before the injection without the danger of saturating the amplifier, which would not recover quickly enough to monitor the voltage change accurately. Clamping the pulse to the ground until just before the Linac injection pulse, as in the low injection type measurements, will not work because the injection signal is initially very nearly equal to the signal due to the high current pulse, thus, high gain cannot be used. For these reasons, the high current pulse is initiated immediately after the Linac injection pulse. It was found that this current pulse could best be applied directly from a pulse generator since there is too much time jitter and contact chatter inherent in a relay administered pulse.

Figure 1 is a block diagram of the circuit developed to achieve accurate recombination measurements over a wide range of injection levels using the procedures detailed above. The time sequences and approximate pulse shapes obtained are shown in Figure 2.

Circuit diagrams of the gate relay circuit and the voltage pulse relay circuit are given in Figure 3. The relays in both these circuits are Magnareed dry reed relays since this type of relay has a faster and more reproducible response time than either telephone-type or mercury relays.

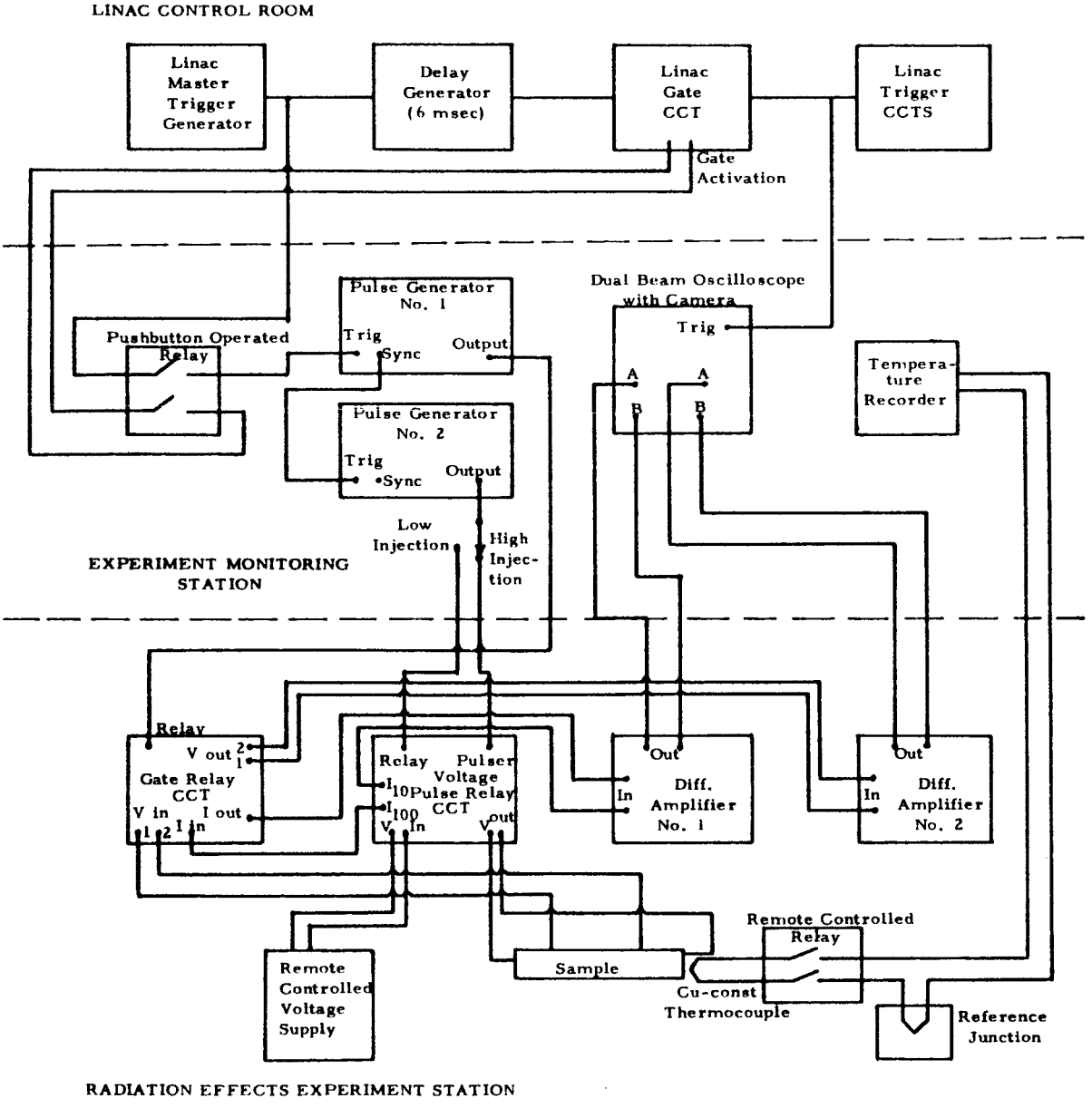

Fig. 1--Recombination measurement circuitry

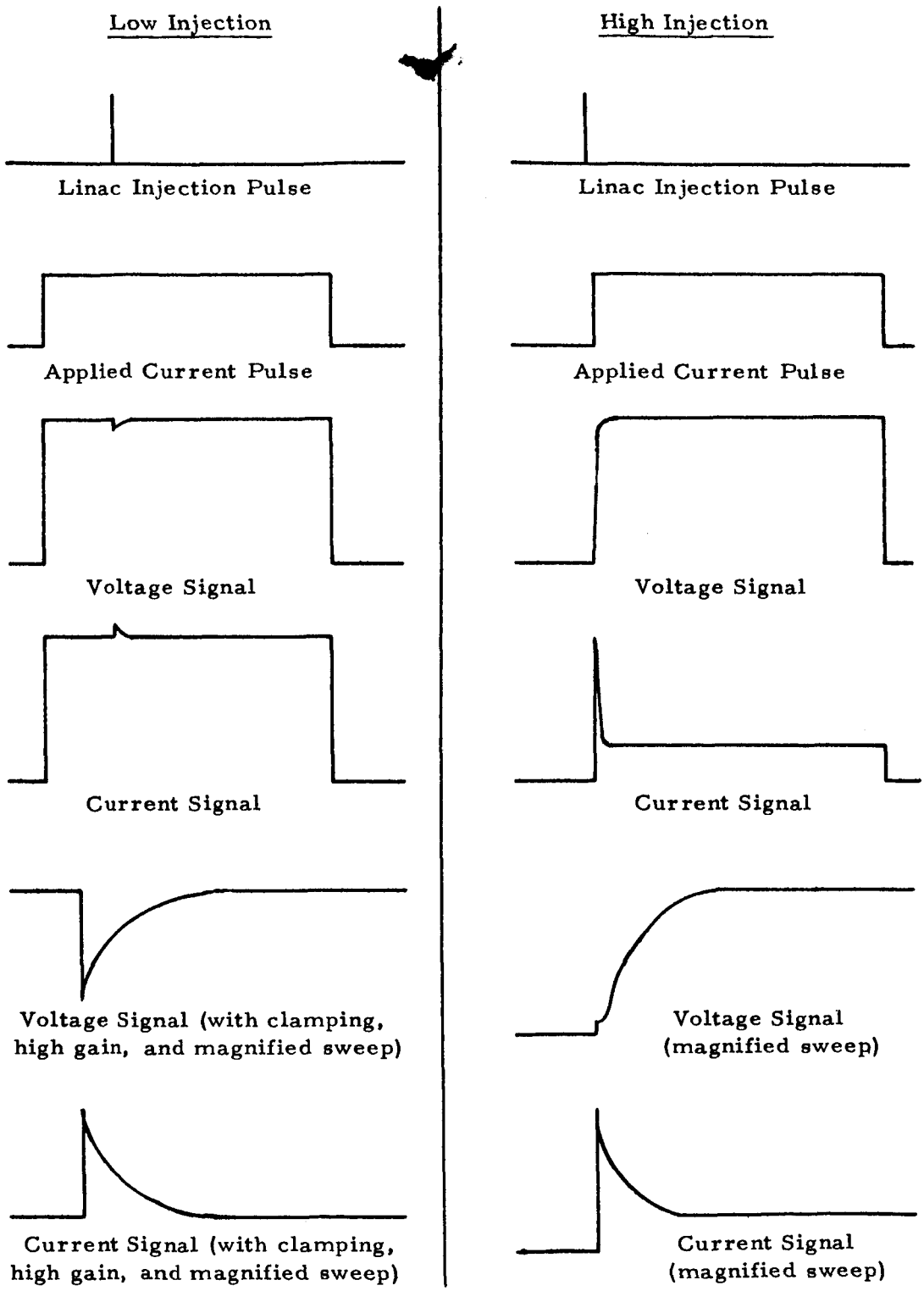

Fig. 2--Approximate pulse shapes achieved during experiment

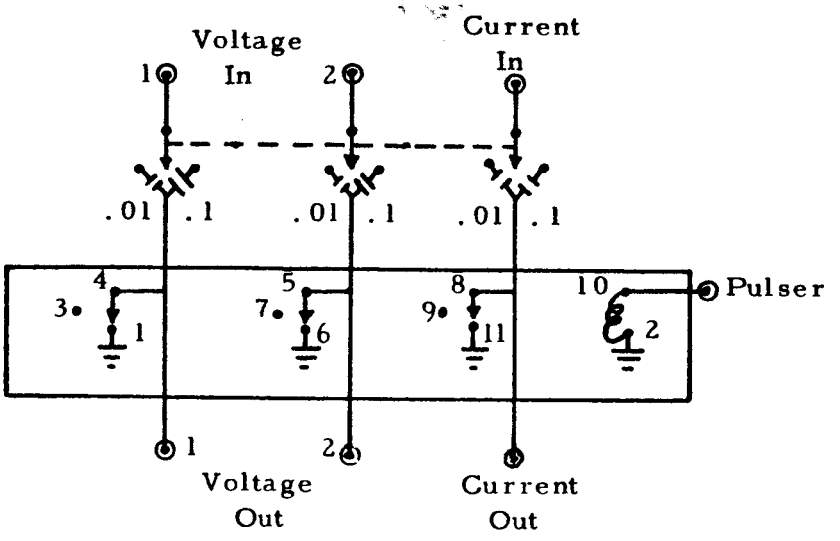

Fig. 3a--Gate relay circuit

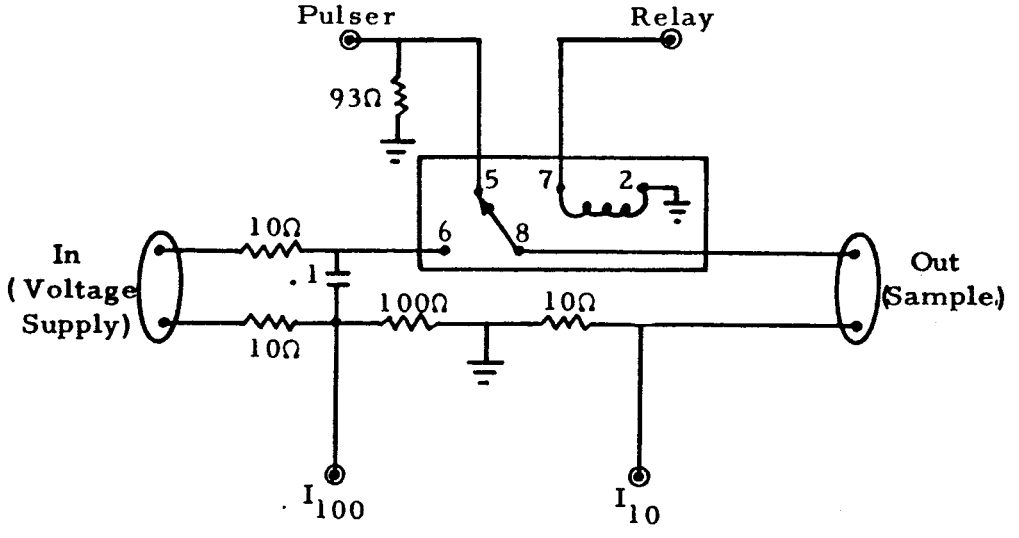

Fig. 3b--Voltage pulse relay circuit

Two Rutherford B7B pulse generators are used to operate the relays in the gate and voltage pulse circuits when investigating low injection level response, and one of the pulsers operates the gate relay while the output of the other is applied directly to the sample under high injection conditions.

The remote-controlled voltage supply is a collection of batteries with the desired output selected through use of a stepping relay. Batteries are used because they are more noise free and are less susceptible to wild transients on switch closure than a dc power supply; they also give a more stable and ripple-free current pulse than a pulse generator.

The differential amplifiers with push-pull output have been described and their characteristics and performance data has been presented previously.[1]

The output of the Cu-Constantan thermocouple is brought out to a Varian Model G-11A strip chart recorder and is continuously monitored during an experiment. The thermocouple is disconnected by a remote controlled relay when pictures of the decay of the excess conductivity are being taken because the long measuring leads act as a pickup for rf noise produced by the Linac.

The changes in current and voltage following carrier injection are observed on a Tektronix 551 dual beam oscilloscope using two Type G differential pre-amplifiers.

The setup for these experiments is shown below.

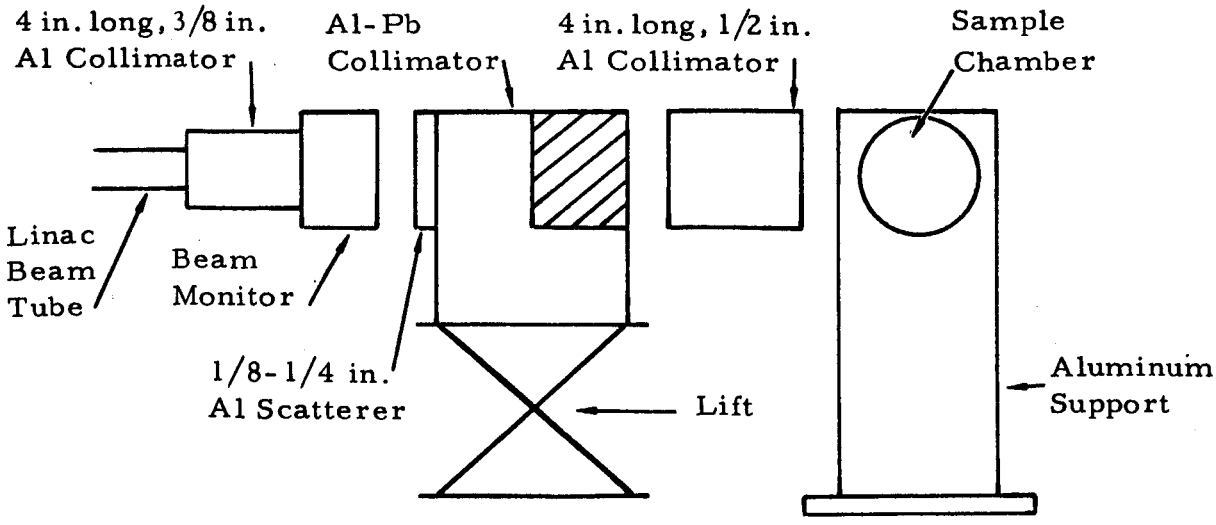

2.3 Data Reduction

The data reduction system has been described previously.[1] During the current research, the same methods were used with minor modifications in the computer program to account for the new methods of applying current to the sample.

2.4 Experimental Results

Successful irradiation experiments have been performed on two 7 ohm-cm n-type floating-zone refined (FZ) silicon samples and one p-type FZ sample. The data from the p-type sample have not been reduced, so only the results of the n-type experiments are reported here.

The purpose of these experiments was to determine in detail whether the dependence of the lifetime on excess-carrier concentration could be described by the Shockley-Read formulation or whether significant deviations were encountered for very high or very low excess carrier concentrations. This analysis applies to the defects acting as recombination centers in both non-irradiated and irradiated silicon material.

Figure 4 illustrates the measurement of excess-carrier recombination time in an unirradiated sample. It can be seen that the data are a very good fit to a straight line relationship on semilog paper for excess carrier concentrations that are either small or large compared with the thermal equilibrium majority carrier concentration; however, the slopes of the lines are slightly different for the two different conditions. The apparent very rapid decrease in excess carriers at very early times in the highest level pulse is not understood and should be investigated further.

The Shockley-Read formulation discussed in a previous report[1] predicts that the dependence of lifetime on excess carrier concentration should have the form in n-type material of

$$\tau(1+\Delta n/n_o) = \tau_{po}(1+n_1/n_o) + \tau_{no}p_1/n_o + (\tau_{po}+\tau_{no})(\Delta n/n_o) \qquad (1)$$

where the customary terminology is used. In particular, the intercept of a linear plot of $\tau(1+\Delta n/n_o)$ versus $\Delta n/n_o$ should give the low injection lifetime

$$\tau_\ell = \tau_{po}(1+n_1/n_o) + \tau_{no}p_1/n_o. \qquad (2)$$

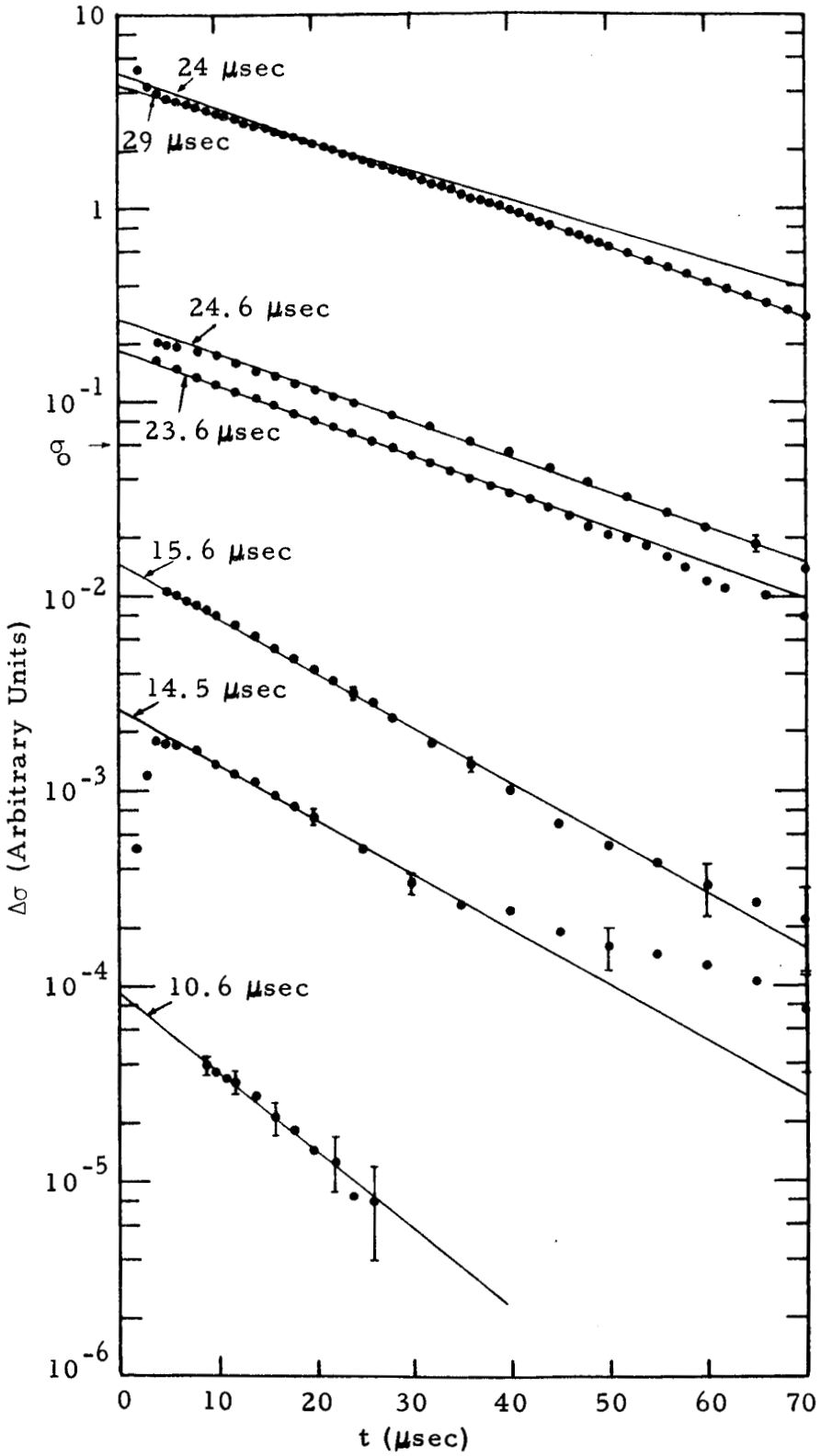

Fig. 4--Recombination in 7 ohm-cm n-type silicon - 295°K

and the slope of the same plot should give the high injection lifetime,

$$\tau_h = \tau_{po} + \tau_{no} \quad . \tag{3}$$

The temperature dependence of the lifetime is usually analyzed on the assumption that τ_{po} and τ_{no} are weak functions of temperature and hence the only temperature dependence resides in the factors n_1/n_o or p_1/n_o. However, this theory predicts that the high injection lifetime τ_h should be roughly independent of temperature. It has been shown previously[1] that even before irradiation the high injection lifetime is as strong a function of temperature as the low injection lifetime.

The slopes of the decay curves in Figure 4 were replotted in Figure 5 to illustrate the agreement between the data and the Shockley-Read formulation. The slope of the line indicates a high injection lifetime of 23 μsec, in reasonable agreement with the value of 24 μsec observed directly at very high injection levels. The somewhat anomalous behavior of the data at an injection level in excess of 20 times the majority carrier concentration is not explained. As shown in Figure 4, the data indicate a rapid decay at early times followed by a somewhat slower decay. This observation seems to be outside the experimental error; however, it should be investigated further before drawing conclusions. Other similar measurements have been performed over a temperature range of 90°K to 386°K. Specifically, one set of data taken at 90°K is illustrated in Figures 6 and 7. It is particularly interesting to note in Figure 6 that the decay of the high injection curve approaches the slope measured in the low injection experiments. The data of Figure 7 represent a silicon sample lightly irradiated, so that approximately three-fourths of the carriers recombine via radiation-induced recombination centers. Similar data from the same sample, taken after irradiation which was heavy enough to produce most recombination via the radiation-induced recombination centers, are illustrated in Figures 8 through 10. The analyses of these data are summarized in Table 1

Table 1

LIFETIMES IN IRRADIATED 7 OHM-CM n-TYPE SILICON

T (°K)	τ_ℓ (μsec)	τ_h (μsec)	τ_h/τ_ℓ
295	0.44±.05	2.2 ±.3	5.0±0.7
386	0.85±.2	3.1 ±.4	3.7±1.0
90	0.48±.1	0.58±.15	1.2±0.3

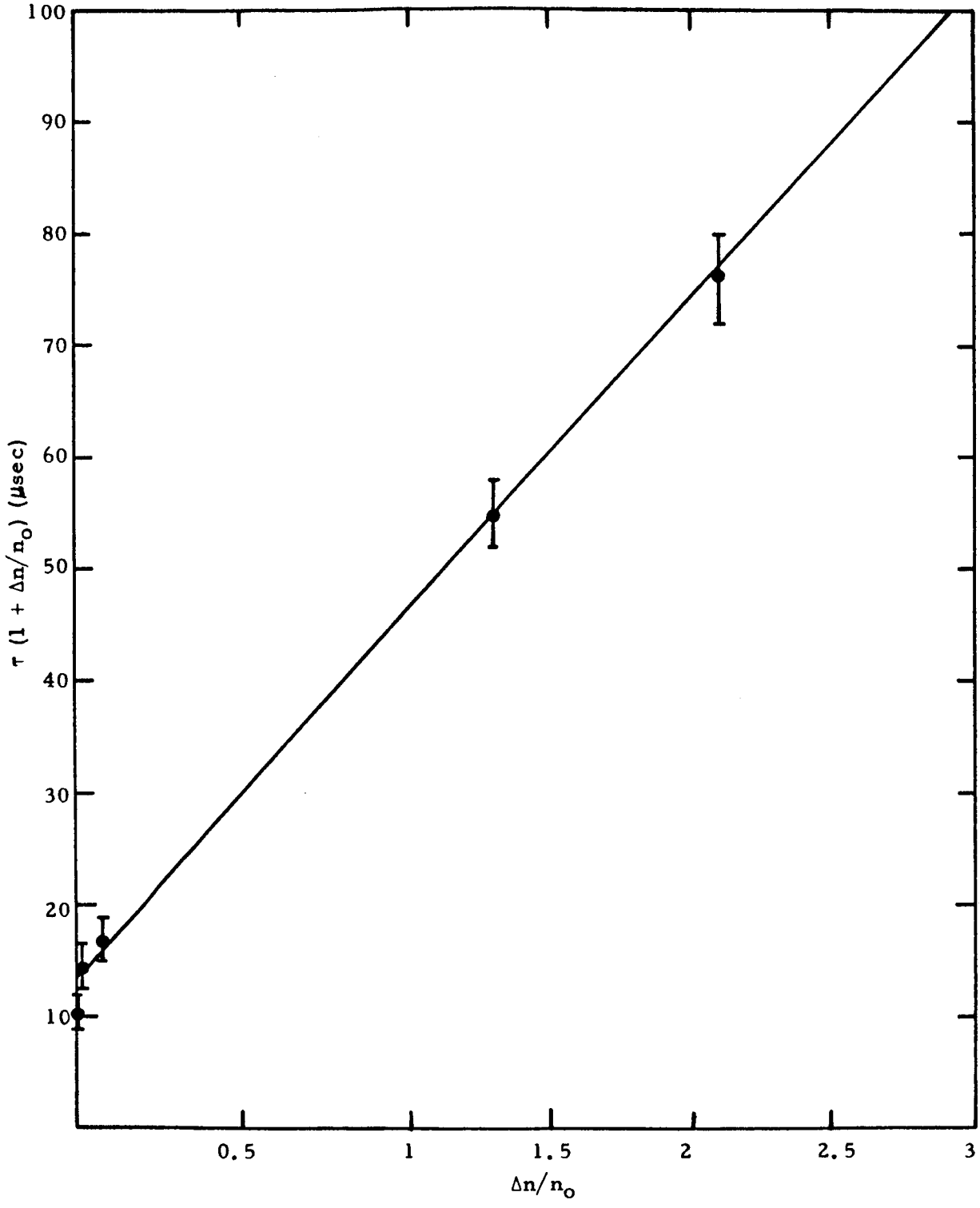

Fig. 5--Dependence of lifetime on excess carrier concentration - 295°K

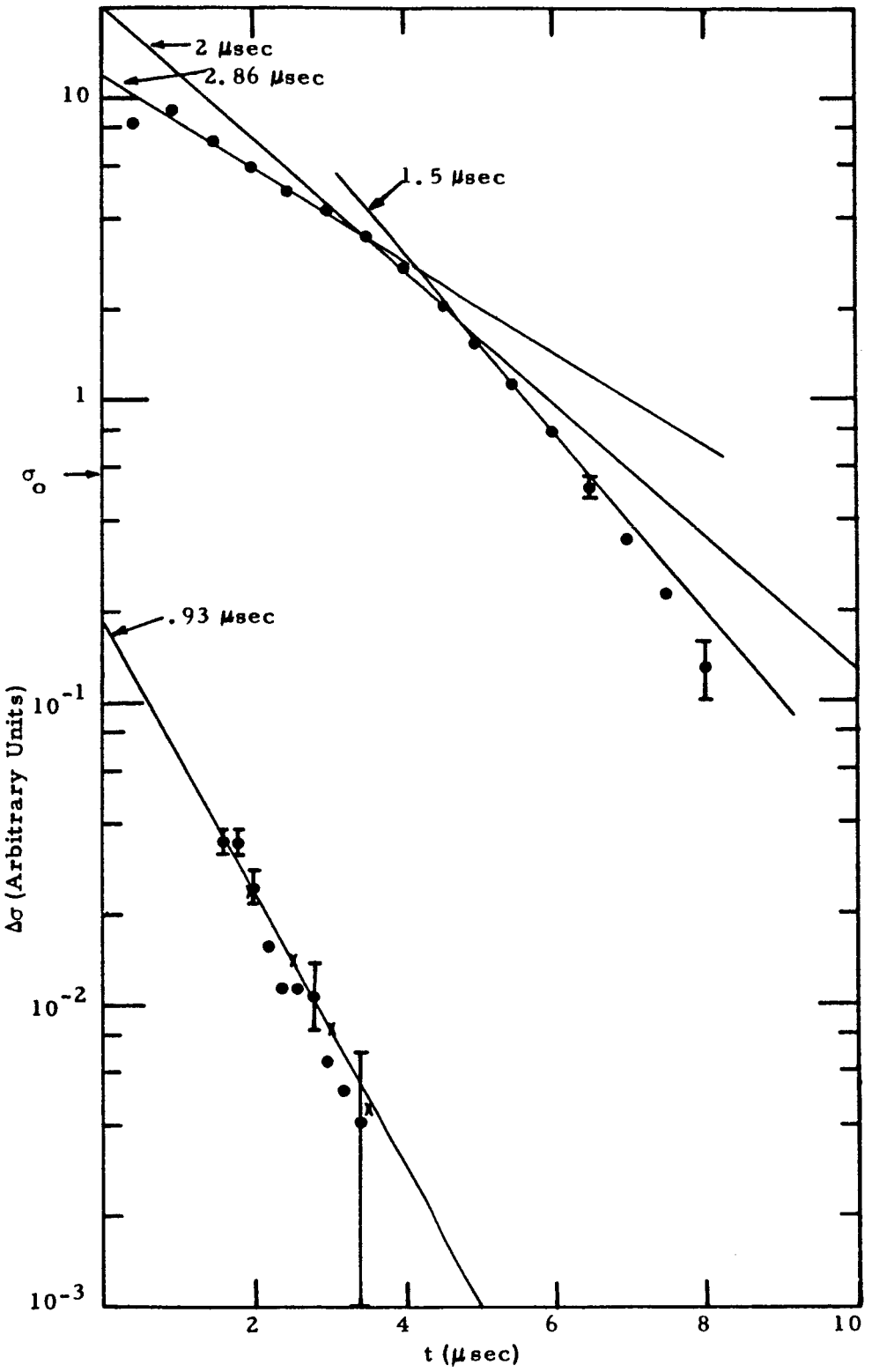

Fig. 6--Recombination in 7 ohm-cm n-type silicon - 90°K

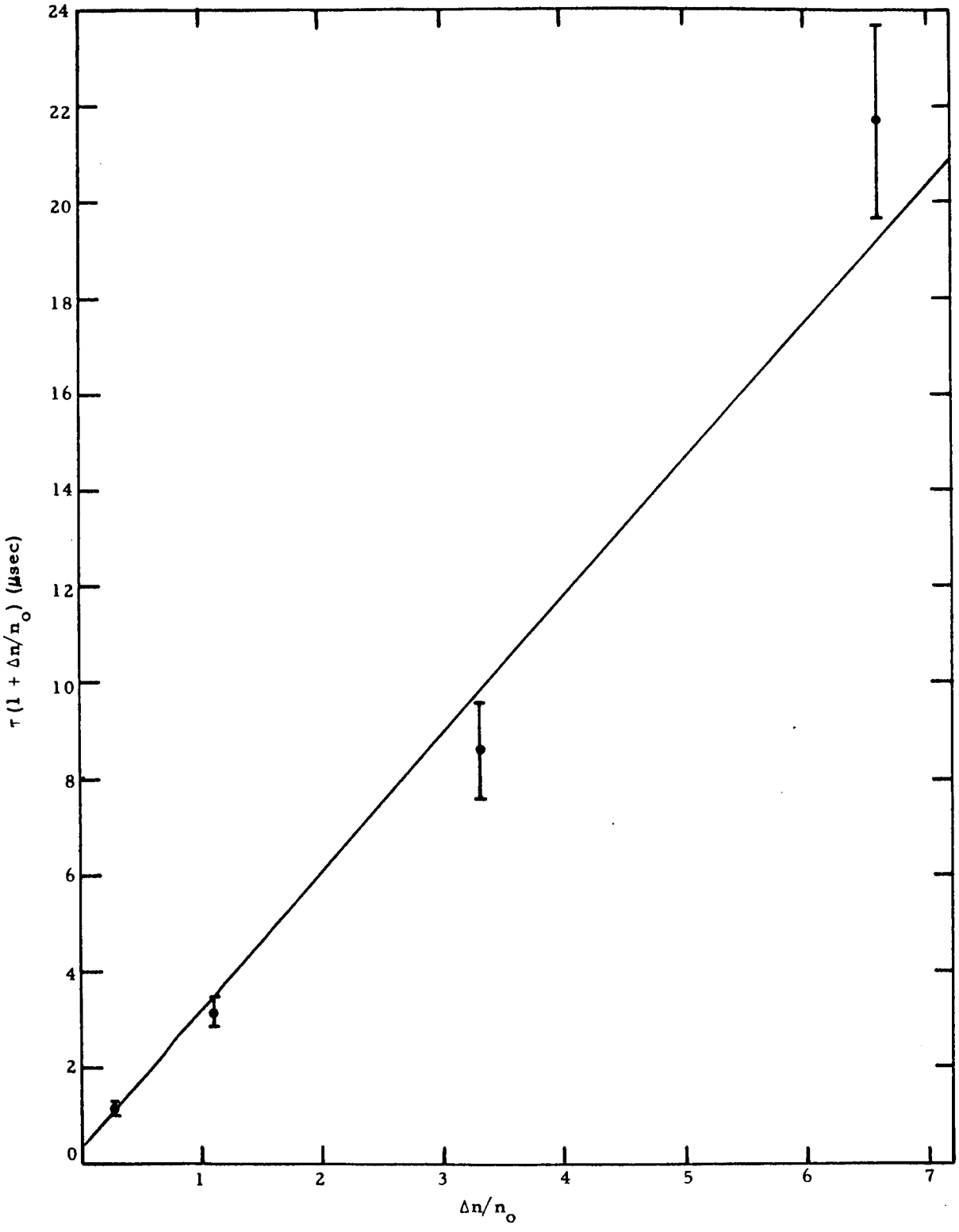

Fig. 7--Dependence of lifetime on excess carrier concentration - 90°K

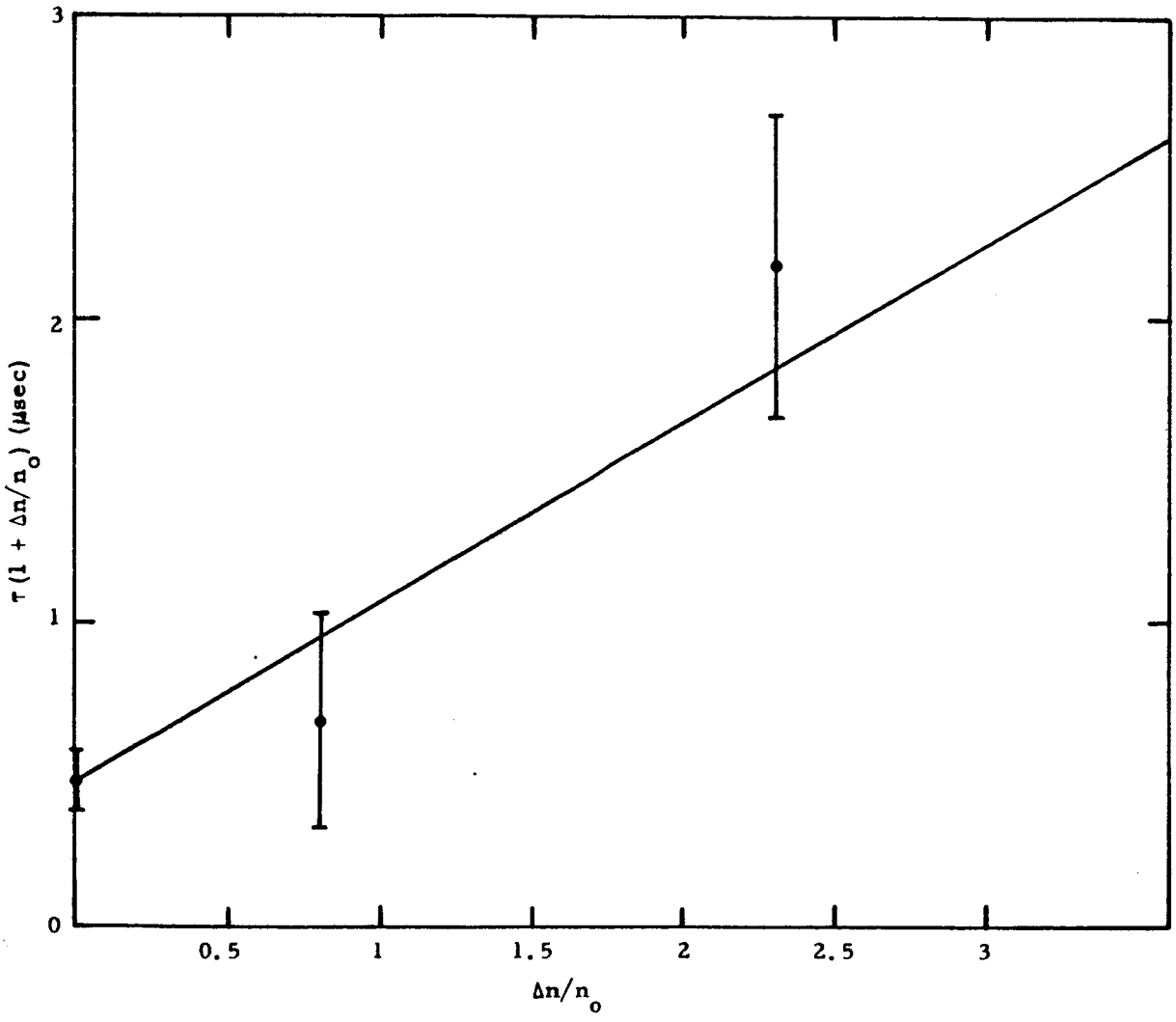

Fig. 8--Dependence of lifetime on excess carrier concentration. Irradiated 7 ohm-cm n-type silicon - 90°K

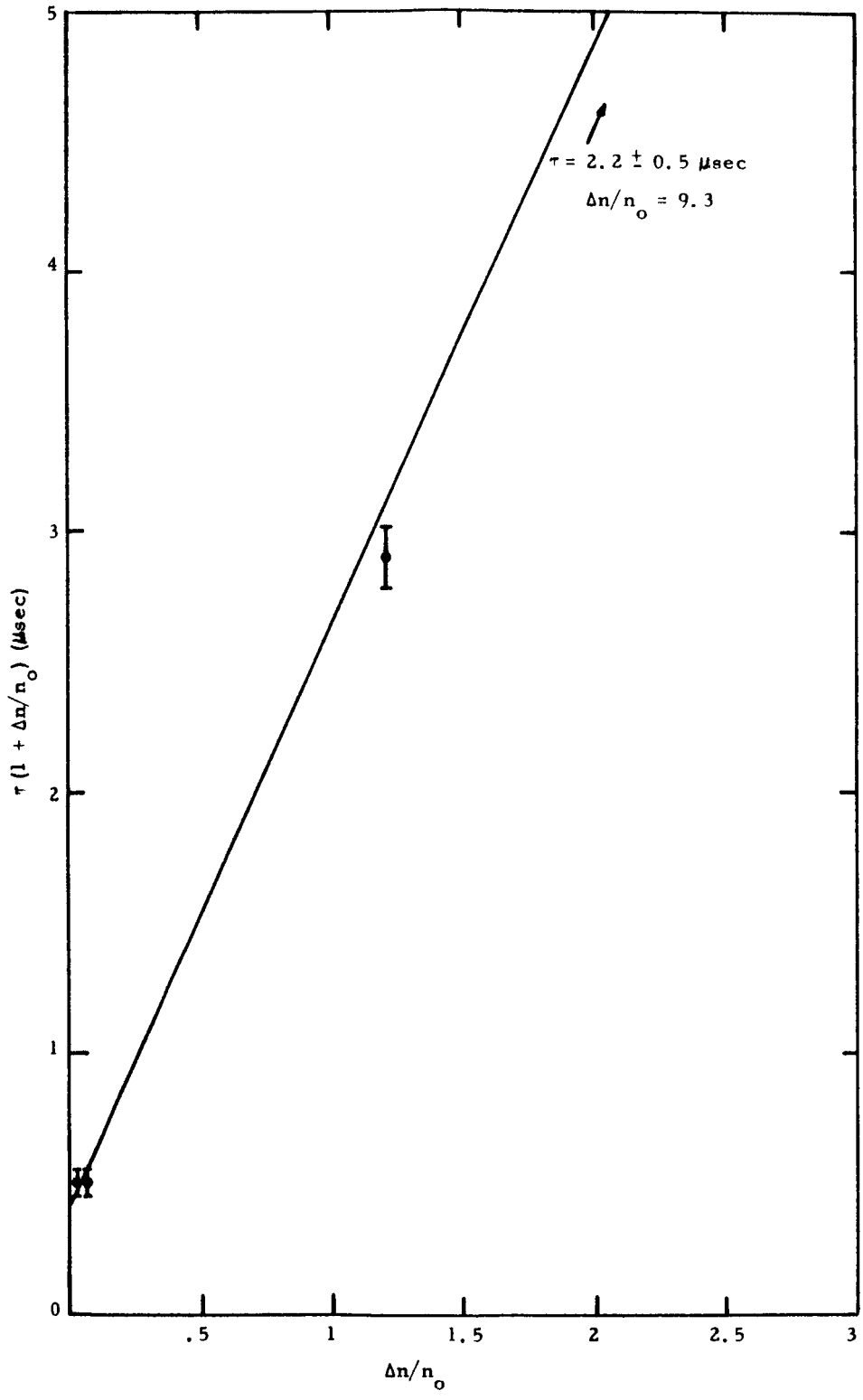

Fig. 9--Dependence of lifetime on excess carrier concentration. Irradiated 7 ohm-cm n-type silicon - 295°K

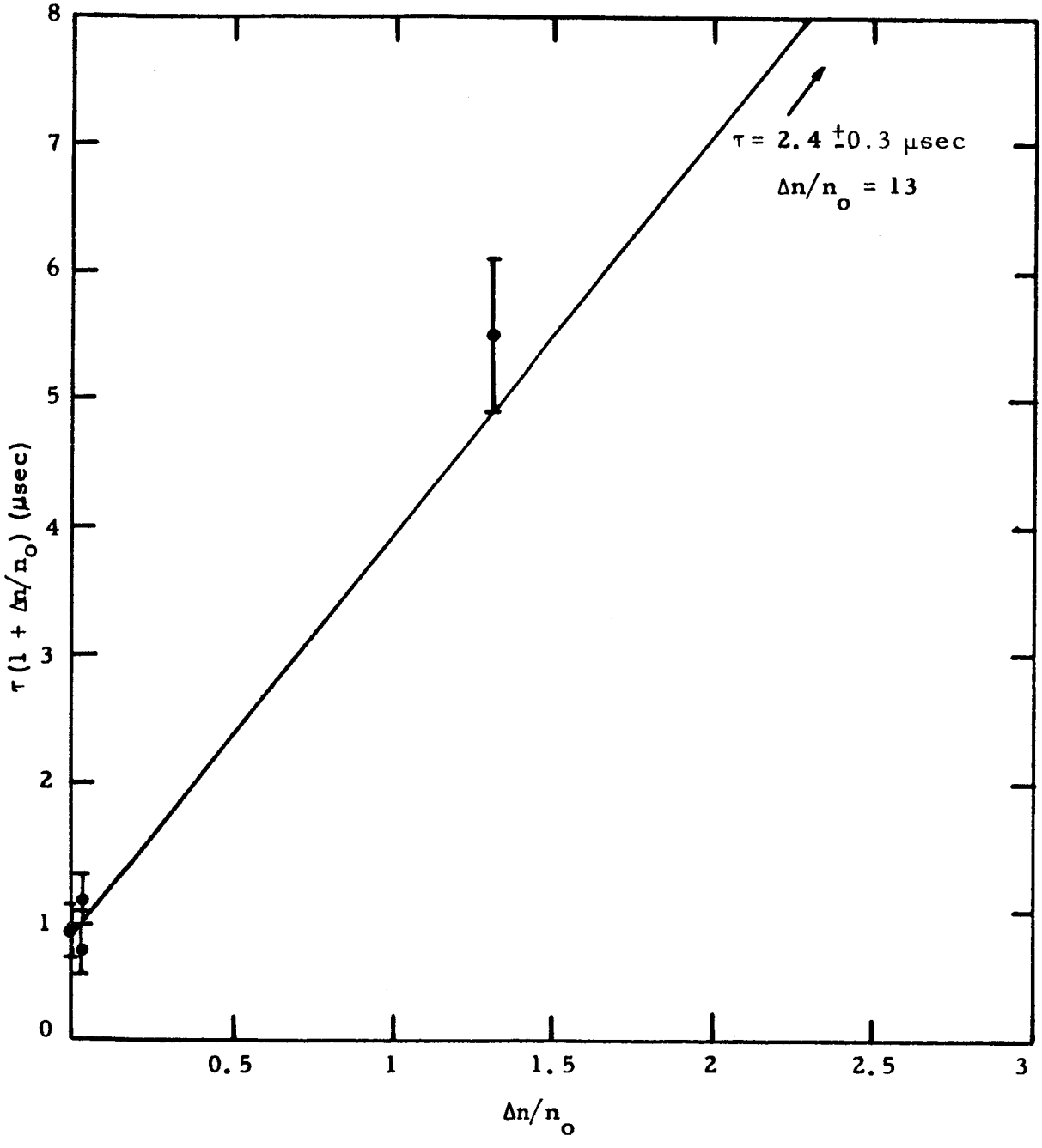

Fig. 10--Dependence of lifetime on excess carrier concentration. Irradiated 7 ohm-cm n-type silicon - 386°K

In the data taken before extensive irradiation, another phenomenon was observed at the limits of experimental accuracy. As seen in Figure 5, the lifetime for the lowest injection level ($\Delta n/n_o = 3.5 \times 10^{-4}$) was slightly smaller than observed at the higher injection levels ($\Delta n/n_o = 1.8 \times 10^{-2}$). This same phenomenon was observed at 376°K as well as 236°K although, at the latter temperature, the lifetime observed at the lowest intensities was longer than the low injection lifetime. In addition, in the temperature range from 128 to 185°K, an appreciable tail having a much longer lifetime was observed after the initial decay. These data are summarized in Table 2, where τ_o represents the lifetime measured at injection levels $\Delta n/n_o < 10^{-3}$. The temperature dependence of these data should be taken with some caution because during this experiment an appreciable amount of displacement radiation effects was produced by the numerous high-injection irradiation pulses, so that it can be assumed that, as one progresses in order down the temperature data in the table, a successively larger fraction of the recombination is taking place via the radiation-induced recombination centers. However, the extent of the damage at a particular temperature is not enough to invalidate the dependence of the lifetime on the injection level.

Table 2

EXCESS CARRIER LIFETIME IN LIGHTLY IRRADIATED 7 OHM-CM n-TYPE SILICON

T (°K)	τ_ℓ (μsec)	τ_n/τ_ℓ	τ_h (μsec)	τ_o (μsec)	τ_{tail} (μsec)
295	13.5 ± 2.0	1.69	23.0 ● 1.5	10.6 ± 1.5	none
376	16.0 ± 1.5	1.3	20.8 ± 1.0 11.6 ± 0.6	10.5 ± 2.0 after irradiation	none
90	0.4 ± 0.1	7.05	2.82 ± 0.4	?	none
128	0.085 ± .02	3.4	0.29 ± 0.07		25 ± 10
185	0.7 ± 0.2	4.3	3.0 ± .15		7 ± 2
236	0.8 ± 0.2	3.25	2.6 ± 0.3		none
375			3.8 ± 0.2		

The interpretation of the tail observed between 128 and 185°K is in terms of minority carrier trapping. This process is observed at excess carrier concentrations $\Delta n/n_o \leq 10^{-2}$, so that it is possible for a relatively small concentration of trapping centers to produce this phenomenon. It has been shown that the decay time of such a tail, if identified with single trapping, should depend exponentially on the reciprocal temperature with a slope given by the ionization energy of the trap. Utilizing these data to calculate the ionization energy, we get a value $E_i = 0.046 \pm 0.012$. Apparently, in this case the trap is the original donor center.

The change in lifetime at extremely low injection levels has a different interpretation. As discussed previously[1] and as reviewed in Section 5 of this report, it can be assumed that the electron and hole concentrations decay independently of each other at extremely low injection levels such that the excess carrier concentration is very small compared to the concentration of recombination centers. Since at these levels our measurement accuracy is noise limited, we expect the measurement to be sensitive primarily to the carrier having the highest mobility, namely the electrons. Hence, in the independent recombination regime, we expect to see primarily majority carrier lifetime. On the other hand, at higher injection levels it has been shown that the recombination process is dominated by the minority carrier lifetime. In particular, according to the Shockley-Read theory, at the very lowest levels the electron lifetime is expected to be $\tau_n = \tau_{no}(1+n_o/n_1)$.

At present, these measurements at the extremely low injection level are not accurate enough to draw conclusions about the validity of this theory and to use them as an extra parameter in the determination of the excess carrier lifetimes. However, it is very attractive to consider this possibility in the future because an accurate determination of τ_ℓ, τ_h, and τ_o at any particular temperature would be sufficient data for a unique determination of τ_{no}, τ_{po}, and n_1 without resorting to any assumptions regarding a temperature dependence of any of these quantitites. To perform these measurements with a minimum of electrical noise interference, it will be necessary to refine the measurement technique slightly. For the present, we will content outselves with an analysis primarily of the lifetimes in irradiated silicon. To begin with, it can be assumed that at 90°K for reasonable values of the ionization energy and concentrations of the recombination center, the terms n_1/n_o and p_1/n_o are negligible compared to one. Hence,

$$\tau_{po} = 0.48 \pm 0.1 \ ,$$

and

$$\tau_{no} = 0..10 \pm 0.18 \ .$$

If one makes the same assumption for the 295°K data, the value of τ_{po} is the same within the experimental error, but $\tau_{no} = 1.8 \pm 0.3$ μsec. If one assumes that n_1/n_o is not negligible at 295°K, the required value of τ_{no} can increase to 2.2 ± 0.3. It is thus clearly demonstrated that the cross section for electron capture by the defect is strongly temperature dependent. At 386°K the alternatives are $\tau_{po} = 2.3 \pm 0.5$, if n_1/n_o is small, or $\tau_p = 3.1 \pm 0.4$, if n_1/n_o is large compared to one. Again, it can be seen that the data between 295 and 386°K are inconsistent with a constant τ_{no} because it is impossible for n_1/n_o to be comparable to one at 295°K without being even larger at the higher temperature. The data are not inconsistent with a temperature-independent value of τ_{po}.

One of the anomalies in the previously reported data[1] is an apparent minimum in the lifetime at temperatures slightly above liquid nitrogen temperature. This phenomena is exhibited by the lightly irradiated sample, as shown in Table 2. The present experiments did not make use of an accurate absolute calibration of the ionization beam, so it is not possible to say with certainty that the longer lifetimes at liquid nitrogen temperature are not due to carrier trapping. However, the earlier experimental results[1] ruled out this interpretation and there is no reason to expect the present results to be appreciably different.

3. ELECTRON SPIN RESONANCE MEASUREMENTS

3.1 Introduction

The usefulness of electron spin resonance (ESR) techniques to identify defects in silicon produced by electron irradiation has been well demonstrated. Watkins[2] and Bemski[3] have reported identification of the A center (oxygen-vacancy pair), the E center (phosphorous-vacancy pair), the divacancy, and the isolated vacancy. In addition, other resonance signals have been seen but are not yet identified. Work reported to date has been on centers produced by irradiation at 1.5 Mev and below, with the exception of some work reported by Bemski at electron energies up to 6 Mev on divacancy production. Because of the energy dependence of radiation-induced changes in the galvano-magnetic properties of silicon, one would also expect to observe differences in the production rates and, possibly, in the types of centers produced as a function of energy of the irradiating electrons. Results of investigation of these possibilities are reported here.

This section covers ESR measurements performed on 0.5 ohm-cm P-doped quartz-crucible grown silicon which had been irradiated at room temperature with 5 Mev and 30 Mev electrons. These measurements were performed at 2.0, 4.2, and 50°K. Due to experimental difficulties, measurements at intermediate temperatures were not possible; however, they are planned for the near future.

In the following sections we shall discuss the experimental setup, outline the types of resonance signals to be expected under various passage conditions, describe the experimental observations and, finally, discuss the conclusions obtained from these observations.

3.2 Experimental Techniques

The microwave spectrometer employs a microwave bridge with superheterodyne detection at 60 Mc. The dc magnetic field is modulated at an audio frequency; the detected output of the i.f. amplifier is amplified at this audio frequency and is finally detected synchronously with the modulation signal. The details of the microwave setup were described in a previous report.[1]

For the present experiments, a rectangular silvered epoxy microwave cavity oscillating in a TE_{101} mode was employed with provisions for inserting cylindrical samples (1/8 in. diameter by 1/4 in. long) along one wall of the cavity in a region of maximum microwave magnetic field. The samples were supported in the microwave cavity between pieces of nylon rod. The sample and nylon rods were inserted into a piece of teflon tubing to hold them together and this assembly is attached in turn to a thin-wall stainless-steel tube (outside of the microwave cavity) which extends out of the cryostat. Studies of orientation dependence of resonance signals are made by rotating this rod and thus the sample; the axis of rotation is along H_1 (the microwave magnetic field) and orthogonal to H_o (the dc magnetic field).

The relative magnitudes of signals and g-values were made by comparison with the known signal obtained from the powdered silicon sample doped with 3×10^{18}/cm phosphorous*. This material exhibits a single narrow homogeneously-broadened line due to conduction electrons. This line (marker) is small and is placed in a position of maximum rf magnetic field in the cavity. The relative magnitudes of the lines being investigated are obtained from a comparison of the appropriate values of signal amplitudes and line widths of the marker and the resonance signal being studied. Similarly, the deviation in magnetic field between these two resonance signals is used to determine the g-value of the unknown.

The cavity filling factor for the test sample was determined experimentally by measuring the resonance signal from a second thin piece of powdered P-doped silicon marker sample containing a known number of spins. This marker sample was mounted in the Teflon tube on one side of the test sample. The magnitude of the resonance signal was measured both with the marker between the test sample and the cavity wall and with the sample combination rotated so that the marker sample was on the opposite side of the test sample (i. e., with the test sample between the cavity wall and the marker). From the signal magnitudes in these two orientations the magnitude of the microwave magnetic field H_1 at the two marker positions was determined, and thus, the value of H_1^2 averaged over the sample was obtained. It was found that $< H_1^2 >_{sample} = 0.67 (H_1^2)_{max}$ $\pm$ 20 percent.

The cryostat used for the present measurements is a metal double dewar suitable for use with liquid N_2, H_2, and He. Provision is included for pumping on the coolant to obtain a range of temperatures with each coolant. The microwave cavity is contained in a thin-walled stainless steel can in order to exclude the coolant from the cavity. This prevents changes in the resonant frequency of the cavity due to the dielectric constant of the liquid and, in addition, eliminates the more troublesome

*We are indebted to Prof. G. Feher for having supplied this sample.

noise caused by bubbling of the coolant. The sample and cavity are cooled by He exchange gas contained within the stainless steel can. The combination of the enclosed cavity and waveguide assembly and the sample mounted on a rod extending out of the cryostat permits changing of samples during a run with a single filling of coolant. The principle drawback of this arrangement is the limited sample volume, which decreases the ultimate sensitivity. Larger sample volumes have not been employed in the present study, but may be necessary for investigating signals from centers present in low concentration.

3.3 Theory

The motion of a set of free spins in the presence of a static magnetic field $\vec{H}$ may be described in terms of the magnetization $\vec{M}$, which they produce, by the usual expression for the precession of a magnetic moment under the influence of an applied field.

$$\frac{d\vec{M}}{dt} = \gamma \vec{M} \times \vec{H}; \tag{4}$$

note that for a spin system with angular momentum $\hbar \vec{I}$, the magnetization is given by $\vec{M} = \gamma \hbar \vec{I}$, where γ is the gyromagnetic ratio. To describe the interaction of the magnetization with its surroundings, we assume that the magnetization decays exponentially towards its equilibrium value M_o along the direction of the applied magnetic field (taken in the z-direction) with a time constant T_1, and that the x and y magnetization components decay exponentially toward zero with a time constant T_2. Including these effects, we find

$$\frac{d\vec{M}}{dt} = \gamma \vec{M} \times \vec{H} - \frac{M_x \vec{i} + M_y \vec{j}}{T_2} - \frac{(M_z - M_o)\vec{k}}{T_1}, \tag{5}$$

where $\vec{i}$, $\vec{j}$ and $\vec{k}$ are unit vectors in the x, y and z directions. Equation (5) is the famous Bloch equation which has had excellent success in describing the behavior of spin systems in the presence of dc and rf magnetic fields, in spite of the phenomenological nature of its derivation.

To include the effect of an rf magnetic field $H_{rf} = H_x = 2H_1 \cos \omega t$ in the Bloch equation, one works in a frame of reference rotating at ω. In this frame, the z component of the magnetic field is $H_o + \omega/\gamma$ (H_o is the dc field in the laboratory system), and the rf field is a constant, H_1. (We neglect the counter-rotating component rotating at 2ω in the rotating frame.)

Calculation of the rf susceptibility $\chi_{rf} = \chi' - i\chi''$ is straightforward but somewhat involved.[4] One finds

$$\chi'(\omega) \equiv \frac{\tilde{M}_x}{2H_1} = -\frac{1/2\,\omega_o \Delta\omega T_2^2}{1 + (T_2\Delta\omega)^2 + \gamma^2 H_1^2 T_1 T_2}\,\chi_o\,, \tag{6}$$

and

$$\chi''(\omega) \equiv \frac{\tilde{M}_y}{2H_1} = \frac{1/2\,\omega_o T_2}{1 + (T_2\Delta\omega)^2 + \gamma^2 H_1^2 T_1 T_2}\,\chi_o\,. \tag{7}$$

Here $\tilde{M}_x$ and $\tilde{M}_y$ are the x and y components of the magnetization in the rotating frame, i.e., the components of the magnetization in-phase and out-of-phase with the driving field H_1. In these equations, values of the magnetic field have been written in terms of the corresponding frequency; i.e., $\omega_o = -\gamma H_o$. In addition, $\Delta\omega$ is the deviation of the applied frequency from the resonant frequency: $\Delta\omega \equiv (\omega - \omega_o)$. Figure 11 is a sketch of the frequency dependence of χ' and χ''.

As mentioned above, the usual experimental technique, and that employed here, utilizes a combination of magnetic field modulation with a simultaneous sweep of the dc field through the resonance. For modulation amplitudes that are small compared to the line width, one obtains a signal at the output of the phase sensitive detector which is proportional to the first derivative of either χ' or χ''. These derivatives are shown in Figure 12.

For signals which obey the theory outlined above, it is possible to obtain an expression for the number of spins responsible for the resonance (proportional to χ_o) in terms of measured parameters. For example, consider a signal which is proportional to the derivative of the dispersion, χ'. One finds from Eq. (7) that

$$\chi_o \propto -2\frac{\Delta\omega_{\ell}}{\omega_o} \cdot \frac{\Delta\omega_{\ell}}{\Delta\omega_{mod}}\,S\,, \tag{8}$$

where $\Delta\omega_{\ell}$ is half the line width (see Figure 14), S is the signal amplitude, and $\Delta\omega_{mod}$ is the modulation amplitude (expressed as a frequency: $\Delta\omega_{mod} = \gamma\Delta H_{mod}$). In principle, it would be possible to make an absolute determination of χ_o in terms of the measured parameters. However, because of the difficulty of determing the overall gain of the system, the

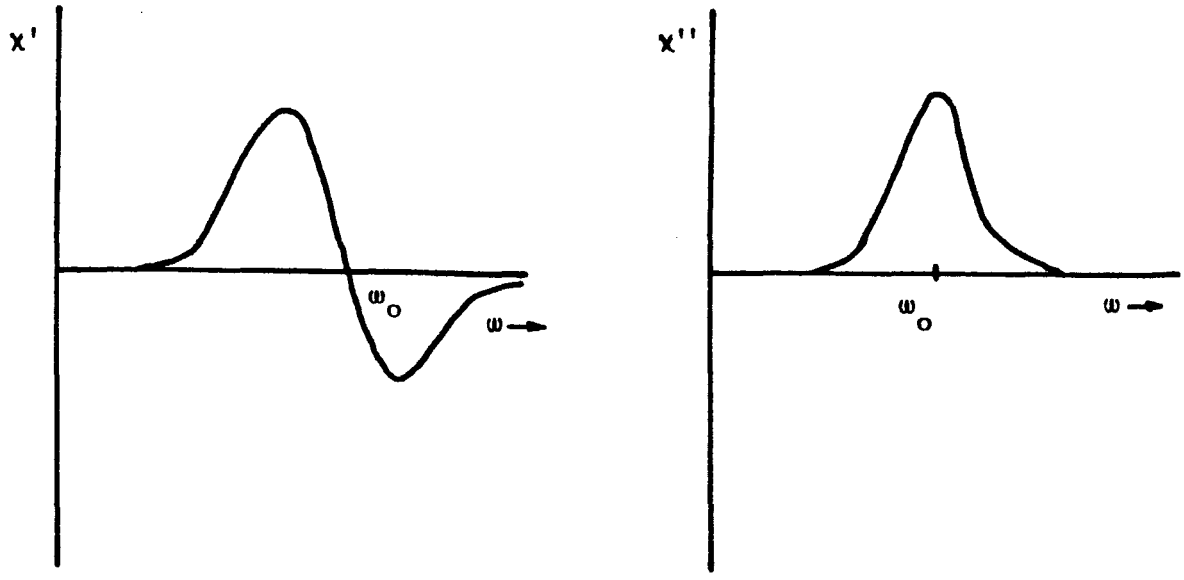

Fig. 11--Real and imaginary parts of susceptibility as a function of field

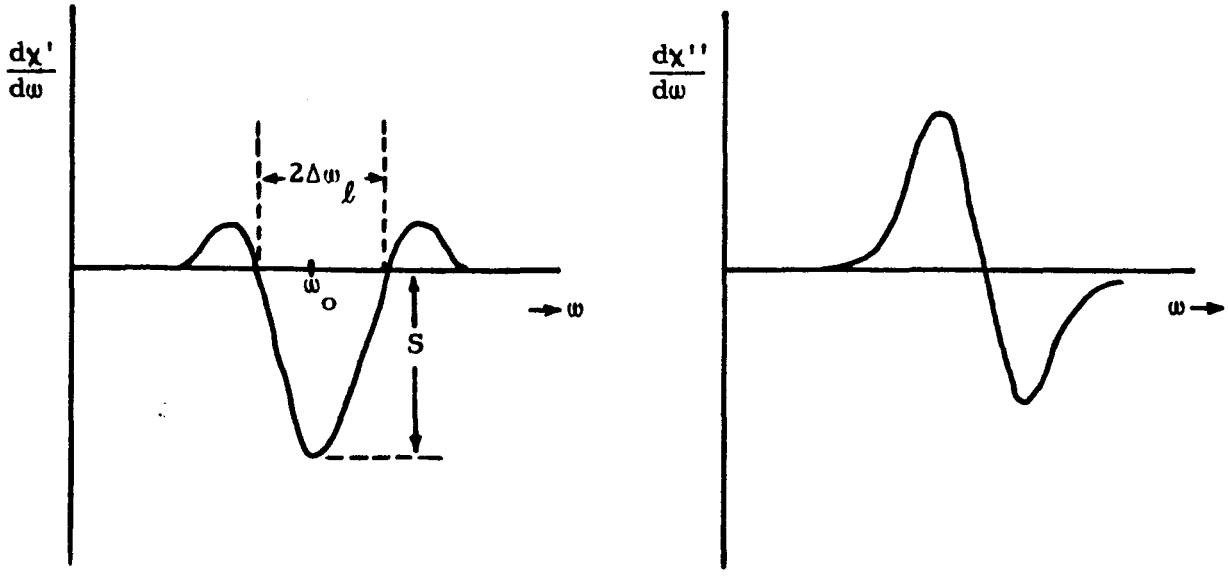

Fig. 12--Derivative of real and imaginary parts of rf susceptibility as a function of field. Measured signal is of this form under slow passage conditions with magnetic field modulation and synchronous detection of signal.

usual procedure, as mentioned above, is to compare the unknown signal with that due to a known number of spins.

The rf susceptibilities obtained from the Bloch equations provide a description of a spin system under what is known as slow passage conditions. In the derivation of χ_{rf}, it was tacitly assumed that the spins were in a steady state configuration with respect to the fields at every point. This will be the case if the line is swept sufficiently slowly. If the sweep rate through the line is too rapid to maintain the steady state configuration, different results will be obtained. These effects are described under the general heading of passage effects. A commonly encountered passage condition is the so-called adiabatic fast passage. In adiabatic fast passage, the resonance is traversed in a time that is short compared to the mean relaxation time $\sqrt{T_1 T_2}$, but slow compared to the precessional frequency of the magnetization. For adiabatic fast passage, the behavior of the magnetization may be easily visualized in the rotating frame. The magnetization sees two components of magnetic field in this frame: $H_o + \omega/\gamma = H_o - H_{rot}$ in the z-direction and H_1 in the x-direction. At a frequency well below the resonant frequency, the magnetic field is essentially H_o and is in the z-direction. (We assume $H_o \gg H_1$). As the applied frequency increases and passes through resonance, the z-component of the magnetic field decreases, passes through zero at resonance, and increases in the opposite direction. The total magnetic field in the rotating frame consequently decreases, rotating in the xz plane to the x-direction and then increases beyond resonance continuing to rotate towards the -z direction. Since this rotation of the magnetic field is slow compared to the precessional frequency (about H_1), the magnetization will follow the field. In addition, since the relaxation time is assumed to be long compared with the time to sweep through the line, no relaxation occurs: the magnitude of the magnetization is constant. Consequently, on making an adiabatic fast passage sweep through the resonance line, the magnetization is inverted. In addition, as we have seen, the magnetization essentially follows the magnetic field. Hence, $\chi_{rf} = \chi'$, and there is no out-of-phase component.

For an inhomegeously broadened line,* Feher[5] has calculated the rf susceptibility for the adiabatic fast passage case. He assumes a Gaussian distribution of resonant frequencies of the line making up the inhomgenously

*By this term we mean a line broadened due to an unresolved splitting of varying magnitudes. Feher has shown the resonance due to donor electrons on phosphorous to be such a line, the splitting being caused by the hyperfine interaction with Si-29 atoms at various distances from the donor nucleus. The resonance lines due to various irradiation-produced centers are presumably broadened similarly.

broadened line and finds for the peak magnitude of the rf susceptibility

$$\chi'(\omega) = \pm\frac{\chi_o}{2}\frac{\omega_o}{\Delta\omega_\ell}\left(\frac{0.69}{\pi}\right)^{\frac{1}{2}}\ln\left(\frac{1.7\Delta\omega_\ell}{\gamma H_1}\right) \qquad (9)$$

For the case of field modulation, one does not simply obtain the derivative of the line shape as in the case of slow passage. This is clear since the modulation causes many successive fast passages through each individual component of the inhomogeneously-broadened line during which the magnetization is inverted and re-inverted many times. For this case, Feher obtains for the component of the rf susceptibility varying at the modulation frequency

$$\chi'(\omega) = \frac{2\chi_o}{\pi}\frac{\omega}{\Delta\omega_\ell}\left(\frac{0.69}{\pi}\right)^{\frac{1}{2}}\ln\left(\frac{1.7\Delta\omega_\ell}{\gamma H_1}\right)\exp\left[-0.69\left(\frac{\omega-\omega_o}{\Delta\omega_\ell}\right)^2\right] \qquad (10)$$

where it is assumed that the line is traversed in a time short compared to the relaxation time. Here $2\Delta\omega_\ell$ is the line-width at half power. Hence, in this case the relative number of spins ($\propto\chi_o$) can also be determined from the peak value of the resonance signal, the width of the line, and from the magnitude of the rf field at the sample (which is determinable from the appropriate cavity parameters and the magnitude of the incident power).

A number of other possible passage conditions are possible, in addition to slow passage and the adiabatic fast passage discussed above. This problem has been considered in considerable detail by Weger[6] who points out, quoting Abragam, that there are seven parameters with dimensions of a frequency relevant to resonance investigations of inhomogeneously broadened lines: $1/T_1$, $1/T_2$, $\Delta\omega_\ell$, γH_1, $\Delta\omega_{mod}$, Ω (the frequency modulation) and $(1/H_i)(dH_o/dt)$. The behavior of the system can depend on the relative value of these various frequencies. Weger has treated eleven separate cases and indicated the expected signals to be obtained with field modulation prior to narrow band amplification and also after synchronous detection. Since no concise summary of his results can be given, it would not be appropriate to discuss his work further at this time. It is clear, however, that an appreciation of the types of behavior possible in the various passage conditions is necessary for appropriate interpretation of experimental results. The results discussed in Section 3.4 were obtained under conditions which meet the conditions for the type of adiabatic fast passage described above or under slightly non-adiabatic conditions (the instantaneous rate of sweeping through the component of the line is slightly faster than the precessing magnetization can follow during part of the modulation cycle). Weger shows, however, that the results for this case are essentially identical to the adiabatic case.

One additional effect has been observed by Feher in connection with his measurements in P-doped silicon; i. e., the signal strength decreases in times much shorter than the spin-lattice relaxation time caused by a decrease in the magnetization. Such an effect can be caused by a dephasing of the spins making up a particular spin packet which contributes to the inhomogeneously broadened line. Such dephasing occurs during a passage of the line. Because a given line is traversed many times by the modulating component of the dc magnetic field during a single sweep of the inhomogeneous line, a considerable reduction in amplitude can occur. This situation is also discussed by Weger. We indicate in Section 3.4 the results of this effect on the resonance signals observed.

3.4 Experimental Results

3.4.1 5 Mev irradiations

A series of quartz-crucible grown silicon samples doped with $10^{16}/cm^3$ phosphorous were irradiated at room temperature with 5 Mev electrons with fluxes of 2.6×10^{15} to 3.8×10^{16} electrons/cm^2. In addition to the resonance signals due to electrons bound to the phosphorous impurity, the only other resonance signals seen in these samples were due to A centers. Measurements were made over a g value range of 1.85 to 2.07. Identification of the A-center resonance was made through the orientation dependence of the nonhyperfine split lines. Figure 13 shows a typical orientation dependence of measurements on sample SiMoP.5NZ1-7 at 50°K. The solid curves are plotted for a g tensor with components $g\left[100\right] = 2.0031$, $g\left[011\right] = 2.0093$ and $g\left[0\bar{1}1\right] = 2.0025$, as reported previously by Watkins.[2]

Table 3 is a compilation of the concentration of spins responsible for the observed signals, calculated assuming no decrease in signal strength due to spin-spin relaxation effects of the type already described. A comparison of the magnitude of A-center signals measured at 4.2 and 50°K shows a decrease in intensity of over a factor of 10 at the lower temperature. In addition, one cannot be certain that the magnitude of the A-center signal measured at 50°K is not also reduced. Finally, there is evidence for a similar reduction of the phosphorous signal in that the observed magnitude in the unirradiated sample is approximately a factor of 3 less than the nominal phosphorous concentration of this series of samples. However, the relative magnitudes of concentrations determined at each temperature should be valid since care was taken to obtain the resonance signal from the different samples under identical conditions of modulation amplitude, modulation frequency, field sweep rate and incident power level.

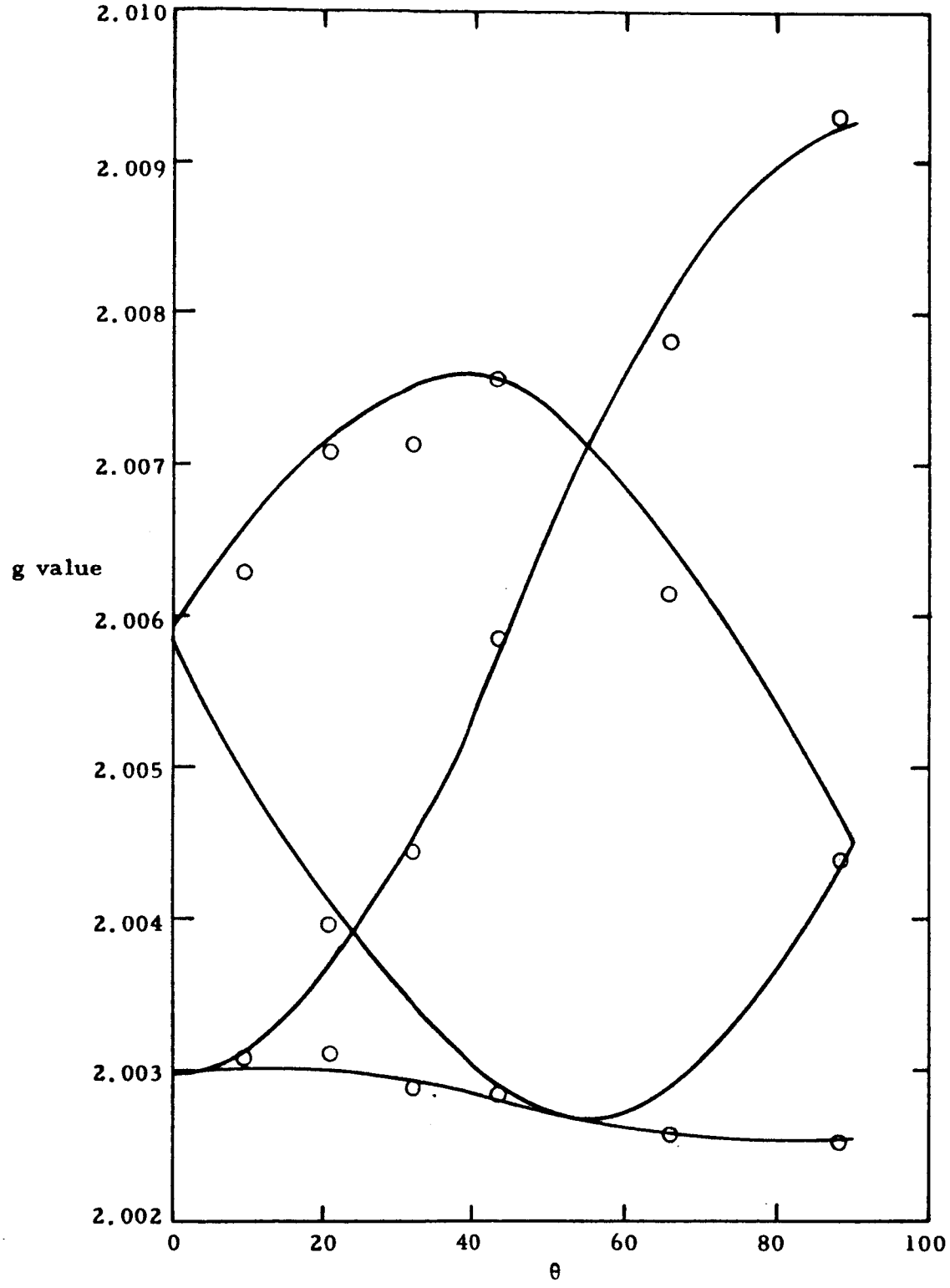

Fig. 13--Angular dependence of g value of A center signal in SiMoP .5NZ1-7. θ is the angle from the [100] direction in a (110) plane.

Table 3

CONCENTRATION OF CENTERS RESPONSIBLE FOR SIGNALS IN VARIOUS SAMPLES IRRADIATED WITH 5 Mev ELECTRONS

Sample	Flux (Electrons/cm^2) ($\times 10^{15}$)	Conc P (cm^{-3})[a] ($\times 10^{15}$)	Conc A (cm^{-3})[b] ($\times 10^{15}$)
SiMoP . 5NZ1-0	0	3.5	
SiMoP . 5NZ7-1	2.6	3.6	
SiMoP . 5NZ1-6	9.2	2.8	
SiMoP . 5NZ1-7	18	1.3	9.3
SiMoP . 5NZ5-1	38	<.2	2.5

[a] Measured at 4.2°K

[b] Measures at 50°K

3.4.2 30-Mev irradiation

Phosphorous doped ($10^{16}/cm^3$) quartz-crucible-grown silicon samples were irradiated with 30-Mev electrons at room temperature over a flux range of 1.9×10^{15} to 1.8×10^{17} electrons/cm^2. The principle resonance signals seen were due to spins on phosphorous impurities and/or A-centers. The concentration of centers responsible for the observed signals are listed in Table 4. The results were calculated assuming adiabatic fast passage conditions with no decrease in intensity caused by spin-spin relaxation effects. The phosphorous signals were measured at 4.2°K and the A-center signals at 50°K. These data are plotted as a function of dose in Figure 14. The error bars shown on this plot represent the possible magnitude of the relative errors for each point. The principal source of error is the noise on the experimental traces of the resonance lines which limits the accuracy with which the magnitude of the peak signal may be determined. Absolute magnitudes are not possible to obtain because of the reduction of signal strengths due to spin-spin relaxation effects. Apart from these effects, the absolute accuracy due to other uncertainties is probably ± 30 percent.

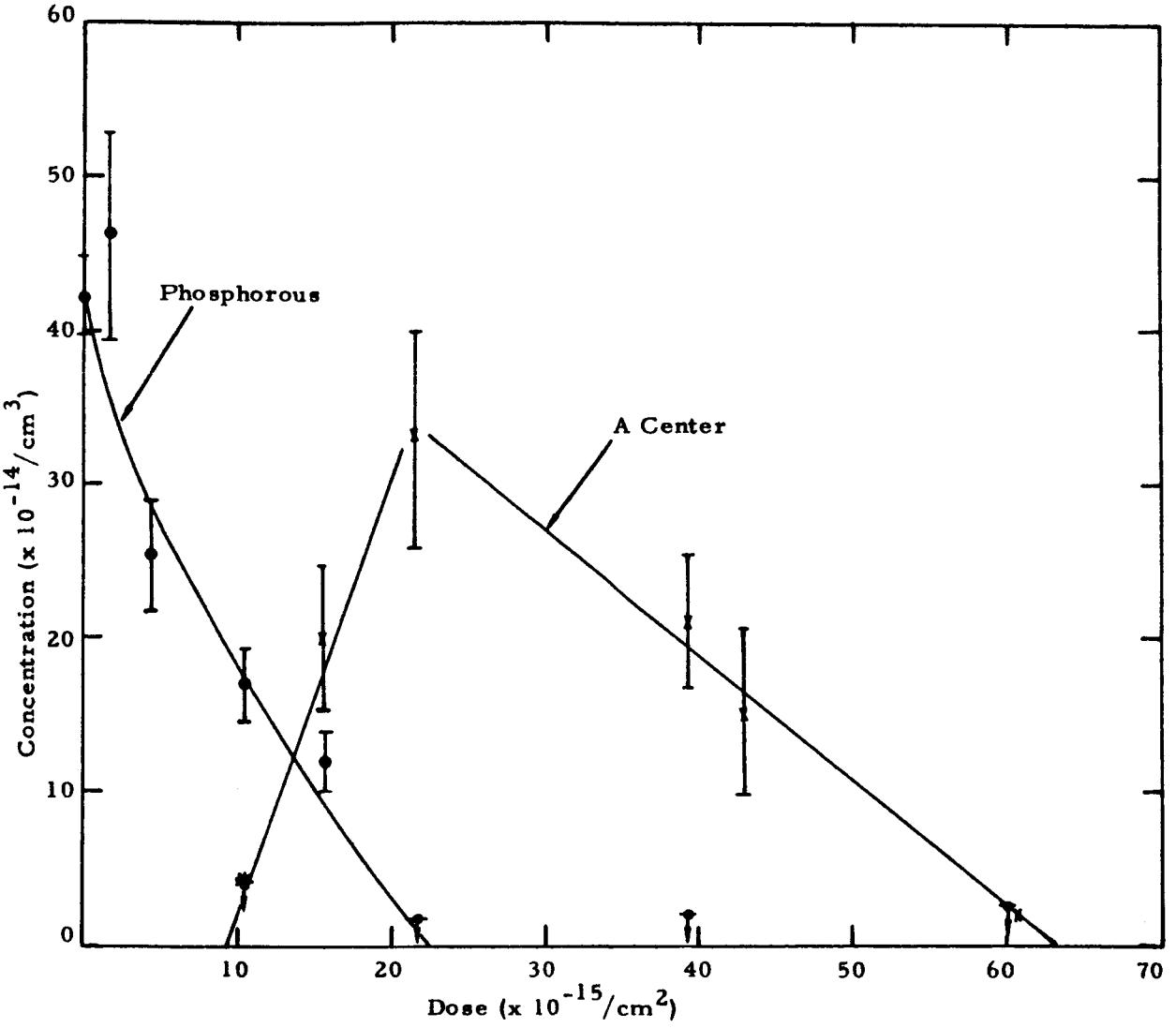

Fig. 14--Measured concentrations derived from phosphorus and A-center spin resonance signals at 30 Mev as a function of dose.

Table 4

CONCENTRATION OF CENTERS RESPONSIBLE FOR SIGNALS IN VARIOUS SAMPLES IRRADIATED WITH 30 Mev ELECTRONS

Sample	Flux (Electrons/cm^2) ($\times 10^{15}$)	Conc P (cm^{-3})[a] ($\times 10^{15}$)	Conc A (cm^{-3})[b] ($\times 10^{15}$)
SiMoP . 6NZ2-6	0	4.2	
SiMoP . 6NZ2-2	1.89	4.6	
SiMoP . 6NZ2-5	4.3	2.5	
SiMoP . 6NZ2-4	10.2	1.7	<.43
SiMoP . 5NZ1-4	15.8	1.2	2.0
SiMoP . 6NZ2-3	21.6	<.18	3.3
SiMoP . 5NZ1-1	39.2	<.20	2.1
SiMoP . 5NZ1-2	43.	not measured	1.5
SiMoP . 5NZ1-5	60.	<.28	1.4
SiMoP . 5NZ1-3	181.	<.46	

[a] Measured at 4.2°K

[b] Measured at 50°K

It must be noted that the data reported here were obtained on samples taken from two different crystals (obtained from the same supplier and nominally identical). As seen in Tables 3 and 4, the phosphorous content measured by ESR in the two materials differed by about 20 percent [SiMoP . 5Z : $3.5 \times 10^{15}/cm^3$; SiMoP . 6Z : $4.2 \times 10^{15}/cm^3$]. This deviation is just outside the limits of the relative errors of these measurements, hence some differences in the materials existed. The effect of this difference on the conclusions expressed below is difficult to judge until additional data on other materials are obtained.

In addition to the above resonance signals, a weak, easily-saturable signal was observed at 4.2°K in samples SiMoP . 5NZ1-1 and SiMoP . . 5NZ1-5 (corresponding to doses of 3.9×10^{16} and 6×10^{16} electrons/cm^2). The g value of this signal is 2.0125 and is apparently isotropic. Assuming adiabatic fast passage conditions and neglecting spin-spin relaxation effects, the magnitude of this signal corresponds to a concentration of $2 \times 10^{14}/cm^3$.

Note that this signal appears at essentially the magnetic field value corresponding to the position of the lower of the two isotropic hyperfine lines of the phosphorous resonance. No signal is seen at the position of the upper line.

Finally samples SiMoP . 6NZ2-4 and SiMoP . 5NZ1-4 (corresponding to doses of 1.0×10^{16} and 1.6×10^{16} electrons/cm^2) were carefully studied for other resonance signals. Within the accuracy of $\sim 1 - 2 \times 10^{14}$/cm^3 available for the sample size used (assuming a line width of $\sim$1 0e) no resonance signals were observed.

3.5 Conclusions

The principle conclusion to be drawn from the present data is that in quartz-crucible grown phosphorous-doped silicon the primary defect produced by electron irradiation at 5 and 30 Mev is the A center, in agreement with previously reported results obtained at 1.5 Mev by Watkins et al.[2] A striking difference between the results of Watkins at 1.5 Mev and our measurements at 30 Mev is the apparent threshold for A center production at 30 Mev. The data on which this observation is based are not extensive, but we believe the conclusion to be valid. The validity of this statement rests on the measurement of an A-center concentration in sample SiMoP . 6NZ2-4 that is less than 2.8×10^{14}/cm^3. Careful analysis of the experimental recorder traces indicates that A centers in concentrations greater than this would have been easily seen. The data thus cannot be explained by a linear dependence of the A center concentration on dose without inclusion of a threshold term. The most probable explanation of this observation is that initially a different center is produced, perhaps by the migration of a vacancy to some impurity or defect other than the oxygen, and an appreciable concentration of A centers begins to form only when this defect is saturated. This suggestion is, of course, highly speculative at this time. Other evidence for formation of a center in appreciable quantities (before A center formation) results from the temperature dependence of lifetime and Hall effect measurements, in which the presence of an energy at 0.12 ev is frequently observed.[1] This energy level and the threshold effect on A center production might be manifestations of the same center. However, to date attempts to observe a resonance signal associated with such a level, and thus appearing at doses below that required for A center production, have not been successful.

The rate of loss of phosphorous signal at 30 Mev is 0.5/cm if we assume that the reduction factor of the phosphorous signal by the spin-spin relaxation effects is 2.4. (This factor increases the concentration of

phosphorous in the unirradiated sample to $10^{16}/cm^3$, the nominal value.) The formation rate of A centers is 0.4/cm and, above the peak, the rate of loss is 0.1/cm neglecting any effects of signal loss due to spin-spin relaxation. This formation rate, which is a lower limit, is more than a factor of 5 greater than the value reported by Watkins et al[2] for irradiation at 1.5 Mev in silicon containing $1.4 \times 10^{16}/cm^3$ phosphorous.

The appearance of resonance signals at doses well beyond that for the peak A center signal has also been reported by Watkins, et al. for 1.5-Mev irradiations.[2] However, since no information was given about these signals, it is not known if they are identical with the g = 2.0125 resonance observed in this work. The apparent isotropic nature of this resonance may indicate, however, that it is not due to a center produced by irradiation but is instead due to an accidental impurity. Further work is in progress to study this resonance.

4. ANALYSIS OF MOBILITY DATA

A new analysis of the Hall data and the change in mobility due to electron irradiation of the silicon samples reported in Table 5 of reference 1 has been made. The parameter of interest is $\Delta n/N_I$, the ratio of carrier (electron) removal (Δn) to the introduction of singly ionized impurities, N_I. This factor is calculated as

$$\frac{\Delta n}{N_I} = \frac{\Delta(1/\mu)/N_I}{\Delta(1/\mu)/\Delta n}, \tag{11}$$

where μ is the mobility. The ratio in the denominator is taken from the experimental data and is given by

$$\Delta(1/\mu)/\Delta n = \frac{\Delta(1/\mu)/\Delta\varphi}{\Delta(1/R_H e)/\Delta\varphi}, \tag{12}$$

where $\Delta\varphi$ is the change in the irradiation flux, R_H is the Hall constant and e is the charge of an electron. The ratio in the numerator is calculated on the basis that the change in mobility is due entirely to the introduction of singly-ionized impurities. Thus the initial value of $1/\mu$ is assumed to have a value due to the combination of the lattice mobility and the ionized impurity mobility μ_I as reported by Long and Myers,[7]

$$\mu_I = \frac{2^{7/2} K^2 (kT)^{3/2}}{\pi^{3/2} e^3 (m^*)^{1/2} N_I \ln(b_1 - 1)}, \tag{13}$$

where K = 12 is the dielectric constant, k is Boltzmann's constant, T is the temperature, $m^* = 0.3\, m_e$ is the electron effective mass, $b_1 = \frac{6 K m^* (kT)^2}{\pi \hbar^2 e^2 n^1}$, $\hbar$ is Planck's constant and n^1 = the number of electron carriers in extrinsic material. The initial value of N_I due to the dopant is taken equal to the number of carriers in the band; that is, the presence of acceptors in the n-type material is assumed to be negligibly small.

The proper way to determine $\Delta(1/\mu)/N_I$ is to calculate μ_I for a given initial value of N_I and for a value $N_I + \Delta N_I$, and to combine these values for μ_I with the known value for the lattice mobility to find the change in the total mobility. The method for combining mobilities in which a

complicated integral is formed has been developed by Debye and Conwell.[8] Dr. Conwell, in a private communication, has stated that the curve in Figure 2 of Reference 9 represents the numerical evaluation of this integral. A plot of $\Delta(1/\mu)/N_I$ versus N_I for silicon at T = 300°K is shown in Figure 15. It is seen from this curve that the common assumption that the total mobility is roughly given by

$$1/\mu = 1/\mu_L + 1/\mu_I, \tag{14}$$

where μ_L is the lattice mobility, is in error, since substitution of Eq (13) into Eq (14) would show that $\Delta(1/\mu)/N_I$ is nearly constant with change in N_I. It should also be noticed that large changes in the calculated value of μ_I do not necessarily imply large changes in the value of the total mobility.

A plot of $\Delta n/N_I$ for fifteen different n-type silicon samples at 300°K is given in Figure 16. The theoretical calculation for μ before irradiation is within 5 percent of the experimental values for μ, but the experimental determination of the small changes in $\Delta(1/\mu)$ is expected to have some error. It is seen that the values of $\Delta n/N_I$ for similar samples of quartz crucible (QC) and floating zone (FZ) samples are identical even though the two types of silicon behaved quite differently in response to different amounts of radiation. It is also apparent that the values of $\Delta n/N_I$ do not change drastically for electron energies of 5 - 30 Mev; however, arsenic and phosphorus doped samples have different types of irradiation defects and the initial amount of doping (resistivity) of the sample is an important parameter in determining the nature of the induced ionized centers.

The value of $\Delta n/N_I$ is not sufficient to identify the types of defects formed; however, the fact that $\Delta n/N_I \neq 1$ shows that defects other than singly-ionized acceptors are formed. When $\Delta n/N_I > 1$, we can expect that some positive ions have changed to negative ions as in the formation of E centers ($\Delta n/N_I = \infty$). When $\Delta n/N_I < 1$, we can deduce the presence of multiply-charged scattering centers, since one multiply-charged ion is a more effective scattering center than an equivalent number of singly-charged defects.

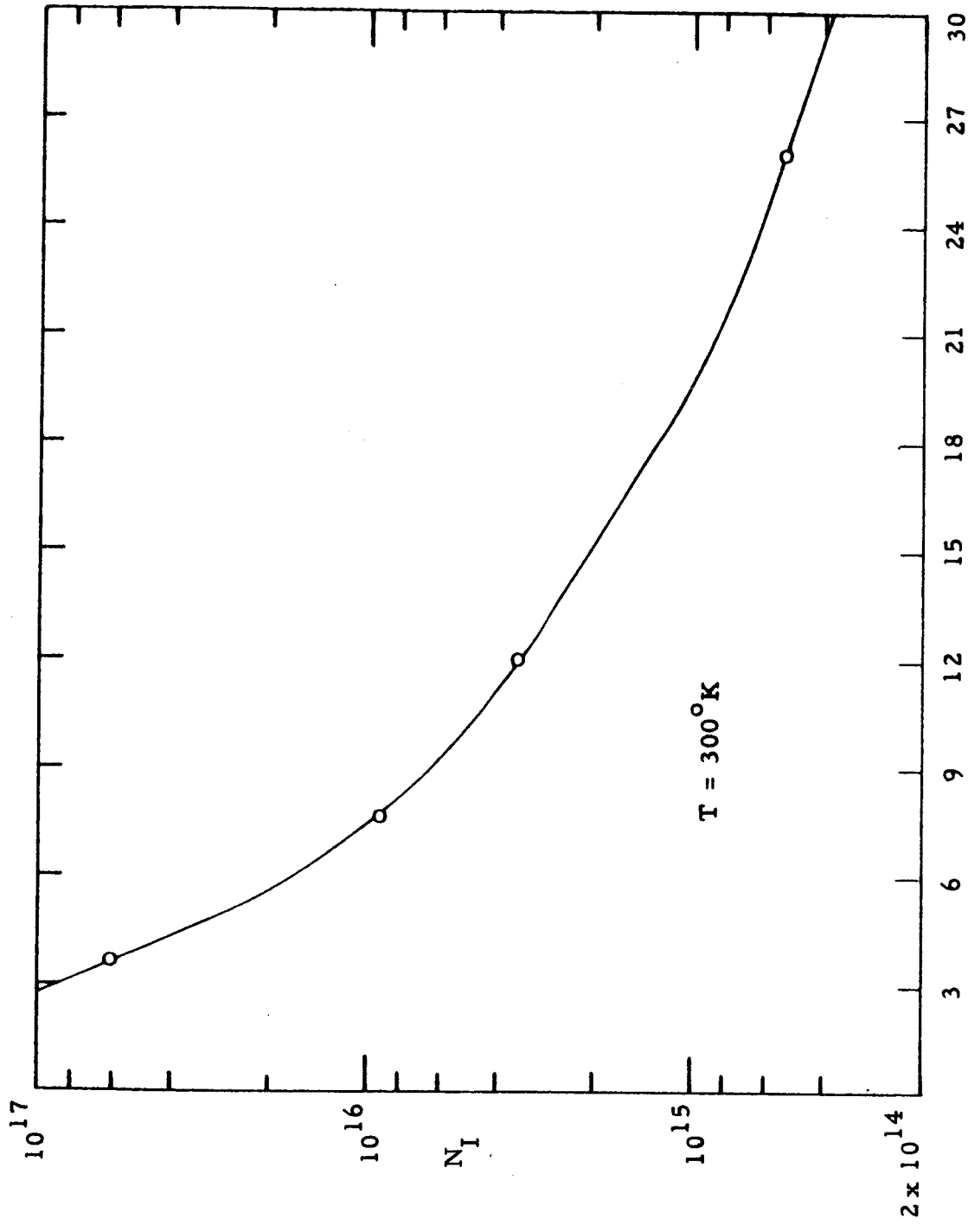

Fig. 15--Theoretical dependence of mobility on ionized impurity concentration

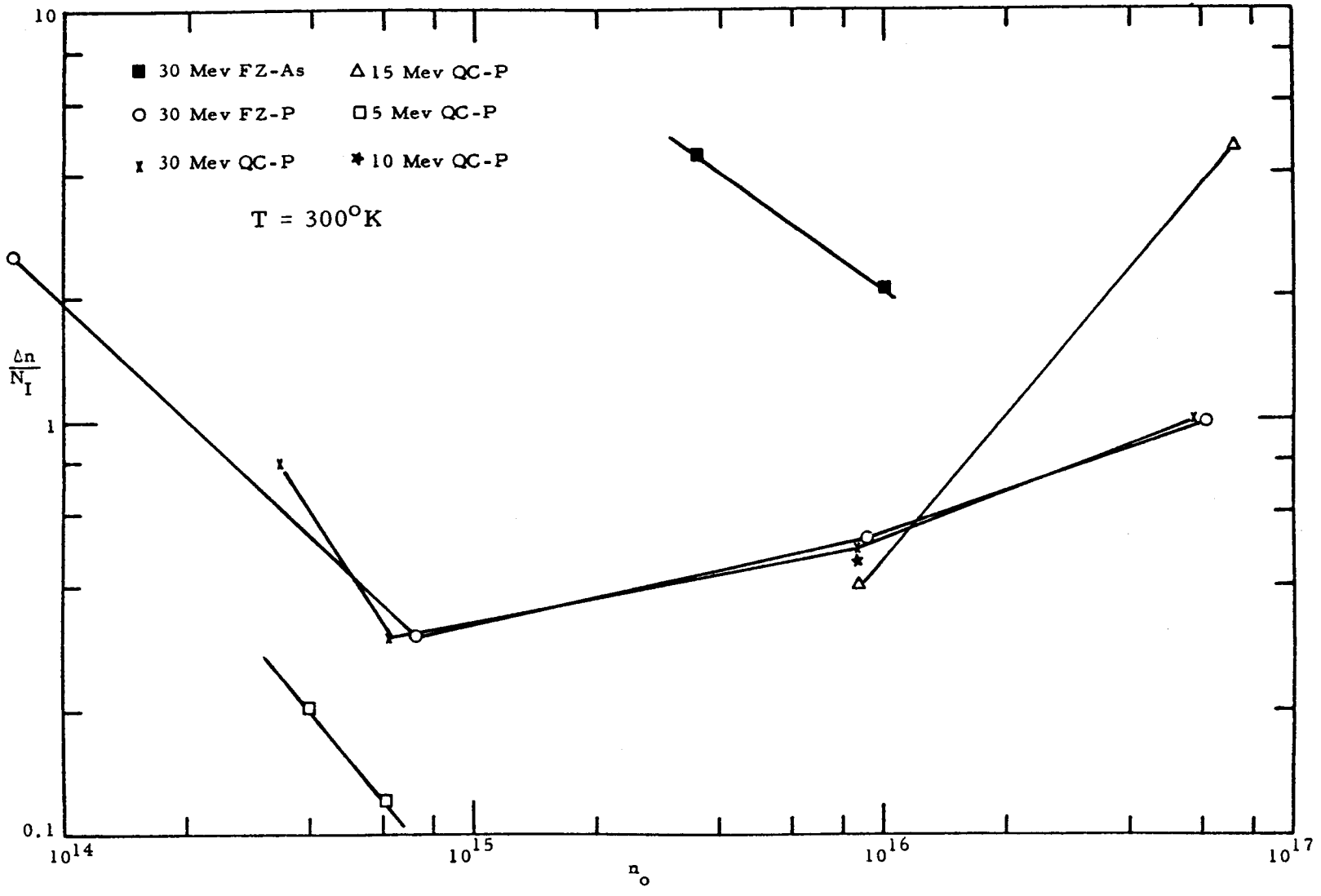

Fig. 16--Comparison of removal rate of carriers with introduction rate of ionized impurities.- n-type silicon

5. STATISTICS OF ELECTRON-HOLE RECOMBINATION FOR A TWO-LEVEL SYSTEM

The statistics of the recombination of holes and electrons in semiconductors is analyzed on the basis of a model in which the recombination occurs by trapping at a defect assumed to have two energy levels in the energy gap. The trap may exist in any one of three states differing by one electronic unit of change. To be exact, we take the trap as +1 when it is empty, +0 (neutral) when it is occupied by one electron, and -1 when it is occupied by two electrons. When the trap is empty, an electron may occupy a level at energy E_2. If this level is occupied, another energy level becomes available for occupancy of electrons at an energy $E_1 > E_2$. The fact that the level at E_1 is only open to electron capture when the level at E_2 is filled distinguishes this system from one in which there are two independent single-level traps whose energy levels are at E_1 and E_2.

The following statistical development parallels and extends the treatment of Shockley and Read[10] which was applied to a single-level system. We introduce the symbol f(E) to represent the probability that a quantum state is occupied where E is the energy level of the state and F is the Fermi level

$$f(E) = 1/\left\{1 + \exp\left[(E-F)/kT\right]\right\} \quad . \tag{15}$$

The ratio of the number of occupied states to unoccupied states is thus,

$$n/p = \frac{f(E)}{1-f(E)} = \exp\left[-(E-F)/kT\right] \quad . \tag{16}$$

If n_2 is the number of electrons at level E_2, n_1 the number of electrons at level E_1, and N_t the number of traps, then from Eq. (16), the ratio of occupied levels available for emptying to the ratio of unoccupied levels available to be filled is, for level E_1

$$n_1/(n_2-n_1) = \frac{f(E_1)}{1-f(E_1)} = \exp\left[-(E_1-F)/kT\right] \quad , \tag{17}$$

and for level E_2,

$$\frac{n_2-n_1}{N_t-n_2} = \frac{f(E_2)}{1-f(E_2)} = \exp\left[-(E_2-F)/kT\right] . \tag{18}$$

The solution of Eqs. (17) and (18) is

$$n_2 = \frac{N_t f(E_2)}{1-f(E_1)\left[1-f(E_2)\right]} , \tag{19}$$

and

$$n_1 = f(E_1)n_2 \text{ or } n_1 = \frac{N_t f(E_1)f(E_2)}{1-f(E_1)\left[1-f(E_2)\right]} . \tag{20}$$

From the principle of detail balancing we require, for each of the two states at equilibrium, a zero net rate of capture and emission of holes and of electrons. (Since the capture of an electron is equivalent to the emission of a hole, we distinguish between electron capture and emission processes as those occurring between the conduction band and an energy level, and hole processes as those occurring between the valence band and an energy level.) We shall denote by $C_{n1}(E)$ the average probability per unit time that an electron in the range dE be captured by an empty trap at energy level E_1; by $C_{n2}(E)$ we denote the corresponding capture probability at E_2. The values C_{p1} and C_{p2} are the capture probabilities for holes at levels E_1 and E_2 respectively. The quantities e_{n1}, e_{n2}, e_{p1}, and e_{p2} are the inverse emission probabilities for each of the capture processes with the same subscripts. The process is shown in the sketch below, where all arrows point in the direction of electron flow.

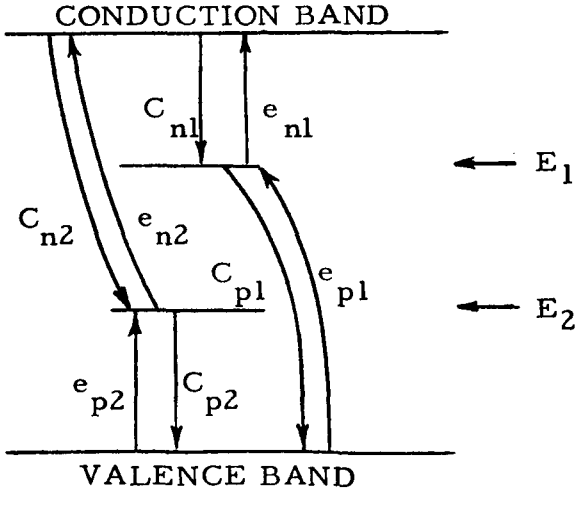

The requirement of detail balance for the electron processes for level E_2 is given by

$$\left\{(N_t-n_2)C_{n2}-(n_2-n_1)e_{n2}\exp\left[(E-F)/kT\right]\right\}f(E)N(E)dE = 0 \qquad (21)$$

where N(E) is the density of electron states in the conduction band. The first term is the capture of electrons into level E_2 which is proportional to the number of empty states at E_2 and to the number of electrons in the conduction band in energy range dE. The second term is emission of electrons into the conduction band which is proportional to the number of available electrons (n_2-n_1) at level E_2 and to the number of vacant states in the conduction band, $\exp\left[(E-F)/kT\right]f(E)N(E)dE$. The equation analogous to Eq. (21) for the level E_1 is

$$\left\{(n_2-n_1)C_{n1}-n_1e_{n1}\exp\left[(E-F)/kT\right]\right\}f(E)N(E)dE = 0 \qquad (22)$$

Solution of Eqs. (21) and (22) gives a relation between the emission and capture cross sections.

$$e_{n2}/C_{n2} = \exp\left[(E_2-E)/kT\right] , \qquad (23)$$

and

$$e_{n1}/C_{n1} = \exp\left[(E_1-E)/kT\right] , \qquad (24)$$

where we have used Eqs. (17) and (18). A pair of analogous equations can be found in the same way for hole processes.

At non-equilbrium conditions, the Fermi-Dirac function f(E) is still applicable if a quasi-Fermi level F_1 and F_2 and F_n is used to specify the occupation of levels E_1, E_2, and the conduction (or valence) band. At thermal equilibrium, the relationship $F=F_n=F_1=F_2$ must apply. The net rate of capture of electrons is then obtained by adding all allowable capture processes and subtracting all allowable emission processes with respect to the conduction band. Thus, if Δn is the number of electrons in excess of the thermal equilibrium number n_o, we have

$$-\frac{\partial \Delta n}{\partial t} = \int dE\left\{(N_t-n_2)C_{n2} + (n_2-n_1)C_{n1} - (n_2-n_1)e_{n2}\exp\left[(E-F_n)/kT\right]\right.$$
$$\left. - n_1e_{n1}\exp\left[(E-F_n)kT\right]\right\}f(E)N(E) ,$$

or, using Eqs. (17), (18), (23), and (24),

$$-\frac{\partial \Delta n}{\partial t} = \int dE \left\{ (N_t - n_2) C_{n2} \left[1 - \exp(F_2 - F_n)/kT \right] + (n_2 - n_1) C_{n1} \left[1 - \exp(F_1 - F_n)/kT \right] \right\} f(E) N(E) \quad .$$

For non-degenerate semiconductors, we integrate to obtain

$$-\frac{\partial \Delta n}{\partial t} = \left(\frac{N_t - n_2}{N_t}\right) \bar{C}_{n2} n - \bar{C}_{n2} n_{a2} \left(\frac{n_2 - n_1}{N_t}\right) + \left(\frac{n_2 - n_1}{N_t}\right) \bar{C}_{n1} n - C_{n1} n_{a1} \left(\frac{n_1}{N_t}\right), \qquad (25)$$

where

$$n = n_o + \Delta n = N_c \exp(F_n - E_c)/kT$$

$$N_c = \int_{E_c}^{\infty} \left[\exp(E_c - E)/kT \right] N(E) dE$$

$$\bar{C}_{ni} = N_t \langle C_{ni} \rangle$$

$$\langle C_{ni} \rangle = \frac{1}{N_c} \int_{E_c}^{\infty} \exp\left[(E_c - E)/kT \right] C_{ni}(E) N(E) dE$$

$$n_{a1} \equiv N_c \exp(E_1 - E_c)/kT$$

$$n_{a2} \equiv N_c \exp(E_2 - E_c)/kT$$

$$p_{a1} \equiv N_v \exp(E_v - E_1)/kT$$

$$p_{a2} \equiv N_v \exp(E_v - E_2)/kT$$

where N_v is the analog to N_c and the other symbols have their usual meanings. A similar development for dn_1/dt, dn_2/dt, and $\partial \Delta p/\partial t$ yields the equations:

$$-\frac{\partial \Delta p}{\partial t} = \left(\frac{n_2 - n_1}{N_t}\right) \bar{C}_{p2} p - \bar{C}_{p2} p_{a2} \left(\frac{N_t - n_2}{N_t}\right) + \left(\frac{n_1}{N_t}\right) \bar{C}_{p1} p - p_{a1} \bar{C}_{p1} \left(\frac{n_2 - n_1}{N_t}\right) \qquad (26)$$

$$\frac{\partial n_1}{\partial t} = \left(\frac{n_2 - n_1}{N_t}\right) \bar{C}_{n1} n - \bar{C}_{n1} n_{a1} \left(\frac{n_1}{N_t}\right) - \left(\frac{n_1}{N_t}\right) \bar{C}_{p1} p + C_{p1} p_{a1} \left(\frac{n_2 - n_1}{N_t}\right) \qquad (27)$$

$$\frac{\partial n_2}{\partial t} = \left(\frac{N_t - n_2}{N_t}\right) \bar{C}_{n2} n - \bar{C}_{n2} n_{a2} \left(\frac{n_2 - n_1}{N_t}\right) - \left(\frac{n_2 - n_1}{N_t}\right) \bar{C}_{p2} p + \bar{C}_{p2} p_{a2} \left(\frac{N_t - n_2}{N_t}\right) \quad . \qquad (28)$$

Equations (25) through (28) are the four equations which govern the carrier concentrations in the traps and in the valence and conduction bands.

5.1 Small Trap Densities

If the trap density is very small compared with the injected carrier density, the different decay rates for the electron and hole densities cannot be sustained for an appreciable time. In the limit of very small N_t' the occupancy of the trap shifts rapidly to a new value so that the rates of electron and hole decay are equal, this process consuming a negligible fraction of the carriers. The above simplification permits solutions of Eqs. (27) and (28) since $\partial n_1/\partial t$ and $\partial n_2/\partial t$ will be very small compared with changes on the right sides of Eqs. (27) and (28). Thus, setting

$$\frac{\partial n_1}{\partial t} = \frac{\partial n_2}{\partial t} = 0$$

for these equations, we obtain values for n_1 and n_2 of

$$n_1 = Gn_2 \qquad G \equiv \frac{n\bar{C}_{n1} + p_{a1}\bar{C}_{p1}}{n\bar{C}_{n1} + n_{a1}\bar{C}_{n1} + p\bar{C}_{p1} + p_{a1}\bar{C}_{p1}} \tag{29}$$

$$n_2 = \frac{(\bar{C}_{n2}n + \bar{C}_{p2}p_{a2})N_t}{(\bar{C}_{n2}n + \bar{C}_{n2}n_{a2} - \bar{C}_{n2}n_{a2}G + \bar{C}_{p2}p - \bar{C}_{p2}pG + \bar{C}_{p2}p_{a2})} \tag{30}$$

Substitution of these values into Eq. (25) gives, after some manipulation:

$$\tau \equiv \Delta n/-\frac{\partial \Delta n}{\partial t} = \frac{\tau_{p2}(n_o+\Delta n+n_{a2}) + \tau_{n2}(p_o+\Delta n+p_{a2}) - G(\tau_{p2}n_{a2}+\tau_{n2}p_o+\tau_{n2}\Delta n)}{(1-G)(n_o+p_o+\Delta n)+\beta/\tau_{n1}}, \tag{31}$$

where

τ is the recombination time,

$\tau_{p2} \equiv 1/\bar{C}_{p2}$,

$$\beta \equiv \tau_{n2}\left(p_{a2} - p_{a2}G_o - n_o p_{a2}\frac{\Delta G}{\Delta n} - p_{a2}\Delta G - p_{a2}n_{a1}\frac{\Delta G}{\Delta n}\right) + \tau_{p2}\left(\Delta n + 2n_o - 2n_o G_o - 2\Delta G n_o - n_o^2\frac{\Delta G}{\Delta n} - \Delta n G_o - \Delta n \Delta G - n_o n_{a1}\frac{\Delta G}{\Delta n} - n_{a1}G_o - n_{a1}\Delta G\right),$$

and

$\Delta G \equiv G - G_o$, where G_o is the value of G at thermal equilibrium.

To compare the recombination time of the two level system with the Shockley-Read recombination time τ_{SR}, we evaluate τ with constants appropriate to the charge states +1, 0, -1 in an n-type semiconductor where two levels are located above the center of the energy gap. The values of the electron crossections σ_{n1}, σ_{n2} and the hole cross sections σ_{p1}, σ_{p2} are proportional to the constants C_{n1}, C_{n2}, C_{p1}, C_{p2} and have the values

$$\sigma_{n1} = 10^{-16}\,cm^2 \quad , \qquad \sigma_{p1} = 10^{-14}\,cm^2 \quad ,$$

$$\sigma_{n2} = 10^{-14}\,cm^2 \quad , \qquad \sigma_{p2} = 10^{-16}\,cm^2 \quad .$$

The expression for G is:

$$G = \frac{1+\Delta n/n_o}{1+\Delta n/n_1+n_{a1}/n_o+\gamma\Delta n/n_o} \tag{32}$$

where $\gamma \equiv \frac{\sigma_{p1}}{\sigma_{n1}} = \frac{C_{p1}}{C_{n1}}$. Thus, at thermal equilibrium

$$G_o = 1/\left\{1+ \exp\left[(E_1-F)/kT\right]\right\} \quad . \tag{33}$$

If E_1 is several kT below F then $n_1 = n_2 = N_t$ at equilibrium. After a dose of radiation ($\Delta n/n_o > 10/\gamma = 0.1$), $G \approx 0$ which reflects the strong attraction of the upper level E_1 for holes. The concentration of each level is independent of the other and the system acts exactly like two single level defects with a recombination time given by

$$1/\tau = 1/\tau_{SR}^1 + 1/\tau_{SR}^2 \tag{34}$$

where the superscripts refer to the energy levels.

If both levels are several kT above F, then $n_1 = n_2 = 0$ at equilibrium. After a dose of radiation, $G \approx 0$, but n_2 increases and the expression for τ becomes

$$\tau = \frac{\tau_{p2}(n_o+\Delta n+n_{a2}) + \tau_{n2}\Delta n}{n_o + \Delta n + (\tau_{p2}/\tau_{n1})(2n_o + \Delta n)} \quad . \tag{35}$$

A plot of $\tau(1+\Delta n/n_o)$ versus $\Delta n/n_o$ is nearly linear as it would be if the lower level were the only recombination mechanism (according to Shockley-Read theory), and the slope is temperature independent.

The greatest departure of the two-level system from the single level system occurs when $E_1 \approx F$. At equilibrium, n_1 is partially full, $n_2 \approx N_t$, and the expression for τ becomes

$$\tau = \frac{\tau_{p2}(n_o+\Delta n+n_{a2}) + \tau_{n2}\Delta n - G(\tau_{p2}n_{a2}+\tau_{n2}\Delta n)}{(1-G)(n_o+\Delta n) + \beta/\tau_{n1}} \quad , \tag{36}$$

where G is given by Eq. (32). A plot of $\tau(1+\Delta n/n_o)$ for three different temperatures is presented in Figure 17, where $n_o = 10^{15}$, $N_\tau = 10^{11}$, $E_1-E_c = -0.256$ ev, and $E_2-E_c = -0.356$ ev. The level for E_1 is the Fermi level for this sample of silicon at 300°K. It is observed that these curves are mildly non-linear and that the slopes have a mild temperature dependence.

5.2 Large Trap Density

If the trap density N_t is so large that the change in trap occupancy is negligible compared with the equilibrium concentrations, then the electron and hole densities decrease independently along the exponential curves with decay times

$$\tau_n = \tau_{n2}\left(\frac{N_t}{N_t-n_{2o}}\right) + \tau_{n1}\left(\frac{N_t}{n_{2o}-n_{1o}}\right) \tag{37}$$

and

$$\tau_p = \tau_{p2}\left(\frac{N_t}{n_{2o}-n_{1o}}\right) + \tau_{p1}\left(\frac{N_t}{n_{1o}}\right) \quad . \tag{38}$$

Here the subscript "o" refers to the values of n_1 and n_2 at thermal equilibrium.

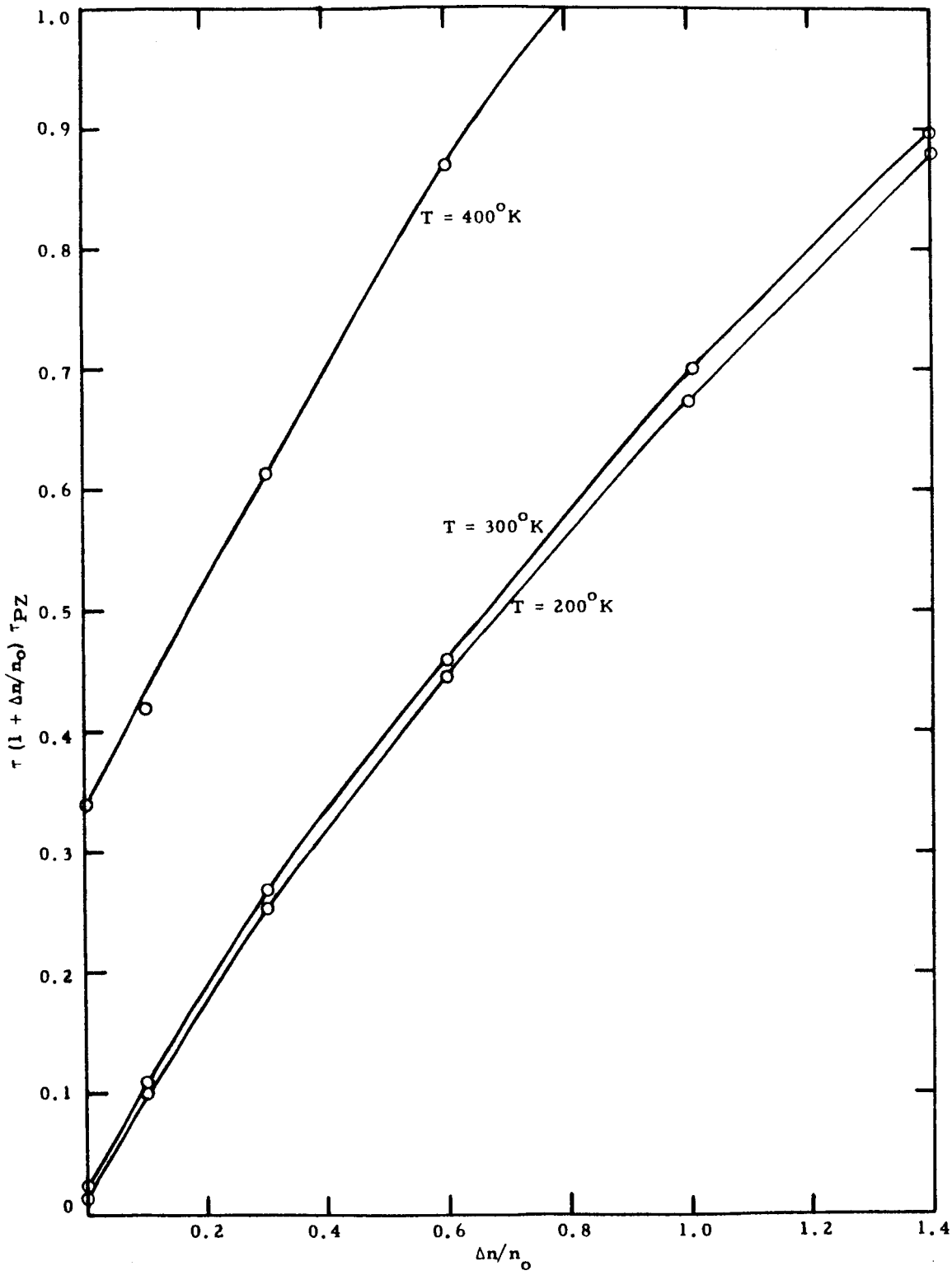

Fig. 17--Predicted dependence of lifetime on excess carrier concentration

6. SUMMARY AND CONCLUSIONS

6.1 Excess Carrier Lifetime Studies

The experimental measurements on lifetime in n-type silicon have indicated the following:

a. The dependence of the lifetime on excess carrier concentration can be adequately described by the single recombination level model of Shockley and Read if one includes a strong temperature dependence for at least the electron capture cross section of the recombination center.

b. A preliminary consideration of a specific two-level system producing the recombination did not reveal an effect strong enough to eliminate the requirement for a temperature-dependent electron capture cross section.

c. The experimental techniques are at the threshold for performing measurements at extremely low injection levels where the electrons or holes are trapped independently. More accurate measurements within this regime could lead to the determination of a third lifetime which would determine the electron and hole capture cross sections as well as the effective density of recombination centers at each temperature independently without requiring a postulate on the temperature dependence of the capture cross section.

d. These measurements should be extended to enable measurement at extremely low injection levels to be performed more accurately.

e. A similar set of data on p-type silicon is being analyzed although such measurements at present are more difficult and correspondingly less accurate because of contact rectification problems.

6.2 ESR Measurements

Spin resonance measurements have been performed on quartz crucible grown silicon doped with $10^{16}/cm^3$ phosphorous and irradiated with 5 and 30 Mev electrons. The only resonance signals definitely identified were those due to spins on the phosphorous impurities and on A centers. The magnitude of the observed resonance signals was uncertain due to loss of magnetization of spin packets during an adiabatic fast

passage through the resonance line. By calibration of the phosphorous signal from an unirradiated sample against the known phosphorous concentration, the loss rate of electrons on phosphorous at 30 Mev was found to be 0.5/cm, in fair agreement with the value 0.6/cm obtained from conductivity and Hall effect measurements. The production of A centers at 30 Mev does not depend linearly on dose unless a threshold term is included below which A-center production rate is very small or zero. This may imply formation of some other center at low doses. No other evidence for such a center was found from spin resonance measurements. The production rate above the threshold is 0.4/cm. Finally, a small, easily saturable, apparently isotropic resonance signal corresponding to g = 2.0125 was observed in samples irradiated at 30 Mev with large doses for which the A-center signal had decreased by about a factor of two below its peak value. This resonance signal has not yet been identified.

6.3 Mobility Analysis

The analysis of the mobility data on silicon irradiated at room temperature reveals the following:

a. For P-doped silicon containing $<10^{16}$ phosphorous atoms/cm^3, we get an effective ionized impurity scattering equivalent to between 2 and 3 singly-charged centers for each net acceptor introduced. For As-doped silicon, on the other hand, the rate of acceptor introduction is greater than the rate of introduction of ionized impurity scattering centers by a factor of 2 to 4.

b. To analyze ionized impurity scattering, it is necessary to have an accurate knowledge of the initial concentration of ionized impurity centers and to take into account the detailed shape of the curve of mobility versus ionized impurity concentration.

REFERENCES

1. van Lint, V. A. J., J. W. Harrity, et al. Radiation Effects on Silicon Solar Cells, Final report on Contract NAS7-91 for the period December 1, 1961 through December 31, 1962. General Atomic report GA-3872. February 15, 1963.

2. Watkins, G. D., J. W. Corbett, and R. M. Walker, J. Appl. Phys. 30, 1198(1959).

   Watkins, G. D.and J. W. Corbett, Phys. Rev. 121, 1001(1961).

   Corbett, J. W., and G. D. Watkins, Phys. Rev. Letters 7, 314 (1961).

   Watkins, G. D., J. Phys. Soc. Japan 18, Suppl. 2, 22(1963).

3. Bemski, G., J. Appl. Phys. 30, 1195(1959).

   Bemski, G., B. Szymanski, and K. Wright, J. Phys. Chem. Solids 24, 1(1963).

4. See, for instance, A. Abragam, The Principles of Nuclear Magnetism (Clarendon Press, Oxford, 1961), Ch. 3.

5. Feher, G., Phys. Rev. 114, 1219(1959).

6. Weger, M., Bell System Tech. J. 39, 1013(1960).

7. Long, D., and J. Myers, Phys. Rev. 115, 1107(1959).

8. Debye, P. P., and E. M. Conwell, Phys. Rev. 93, 693(1954).

9. Conwell, E., Proc. Inst. Radio Engrs. 40, 1331(1952).

10. Shockley, W. and W. T. Read, Jr., Phys. Rev. 87, 835(1952).